https://doi.org/10.5194/esd-2022-10
Preprint. Discussion started: 25 March 2022

Earth System Dynamics
Discussions

A 20-year satellite-reanalysis-based climatology of extreme precipitation characteristics over the Sinai Peninsula

Mohsen Soltani[1], Bert Hamelers[1,2], Abbas Mofidi[3], Ties van der Hoeven[4], Arie Staal[5], Stefan C. Dekker[5], Joel Arnault[6], Patrick Laux[6,7], Harald Kunstmann[6,7], Maarten Lanters[4]

[1] Natural Water Production Theme, European Centre of Excellence for Sustainable Water Technology (Wetsus), Leeuwarden, Netherlands
[2] Sub-department of Environmental Technology, Wageningen University, Wageningen, Netherlands
[3] Geography department, Ferdowsi University of Mashhad, Mashhad, Iran
[4] The Weather Makers B.V., Burgemeester Loeffplein, 'S-Hertogenbosch, Netherlands
[5] Department of Environmental Sciences, Copernicus Institute, Utrecht University, Utrecht, Netherlands
[6] Institute of Meteorology and Climate Research, Karlsruhe Institute of Technology, Garmisch-Partenkirchen, Germany
[7] Institute of Geography, University of Augsburg, Augsburg, Germany
Correspondence: Mohsen Soltani (mohsen.soltani@wetsus.nl)

Abstract

Extreme precipitation events and associated flash floods caued by the synoptic cyclonic-systems have profound impacts on society and the environment particularly in dry regions. This study brings forward a satellite-reanalysis-based approach to quantify the extreme precipitation characteristics over the Sinai Desert in Egypt, from a statistical-synoptic perspective for the period of 2001-2020. Using the satellite remote-sensing precipitation and a set of climate indices, we characterize the spatiotemporal distribution of extreme rainfall climatologies across the Sinai region. Then, using the reanalysis dataset, the synoptic systems responsible for the occurrence of precipitation events along with the major tracks of cyclones during the wet and dry periods are explored. Our results indicate that the temporal changes and spatial patterns of the precipitation events do not show a homogenous tendency, rather lack of spatiotemporal coherence across the Sinai. Northern parts of the Sinai, unlike other areas, exhibit the highest anomalies (approx. ±45 mm/decade); and the annual rainfall trends indicate a drier-climate in the north at −0.03 mm/decade, while a wetter-climate is observed in the central and southern parts at 0.10 and 0.36 mm/decade, respectively. The Mediterranean cyclones accompanied by the Red Sea -and Persian Troughs are responsible for the majority of extreme rainfall events all-round the year. A remarkable spatial relationship between the Sinai's rainfall and the atmospheric variables of sea level pressure, wind direction and vertical velocity is found. Furthermore, the cyclone-tracking analysis indicates that 125 and 31 cyclones (rainfall ≥10mm/day) either formed within -or transferred to the Mediterranean basin and precipitated over the Sinai during wet and dry periods, respectively; while some (~15% with rainfall >40mm/day) being capable of leading to flash flood in the wet period of the region. This study, therefore, sheds new light on the extreme rainfall characteristics and the dominant synoptic mechanisms over the Sinai region in the eastern Mediterranean basin.

1 Introduction

Extreme precipitation events can have fundamental impacts on society and human wellbeing by causing mortality (Trenberth *et al.,* 2007; Toreti *et al.,* 2010; Wannous and Velasquez 2017; Charlton-Perez *et al.,* 2019), and by causing property and ecological damages (Zhang *et al.,* 2005; IPCC, 2013; Nastos *et al.,* 2013; Boucek *et al.,* 2016). Precipitation extremes are realized as one of the severest natural disasters, among many others (Arnous and Omar 2018). Nevertheless, these events are vital for the water resources of the region especially in the water-limited environments (Peleg et al., 2012; Givati et al., 2019; Levy et al., 2020); however, they also constitute the main trigger of flash floods in arid and hyper-arid areas such as the Sinai Peninsula in Egypt (Ocakoglu *et al.,* 2002; David-Novak *et al.,* 2004; El-Magd *et al.* 2010; Farahat *et al.* 2017; Gado, 2020).

The eastern Mediterranean is one of the main cyclogenetic regions of the Mediterranean basin (Krichak *et al.,* 1997) and globally (Ulbrich *et al.,* 2012; Neu *et al.,* 2013), which in many cases associated with precipitation extremes (Flaounas *et al.,* 2014a, 2014b). As such, most of the heavy precipitation events in this region strongly rely on the presence and frequency of the intense Mediterranean cyclones (Trigo *et al.,* 2002; Kotroni *et al.,* 2006;

https://doi.org/10.5194/esd-2022-10
Preprint. Discussion started: 25 March 2022

Earth System Dynamics Discussions

Pfahl and Wernli 2012; Lionello *et al.,* 2016), accompanied by other precipitation producing-systems at synoptic-scale, sometimes of tropical/sub-tropical origin (Krichak et al. 1997; Hochman *et al.,* 2020).
A multitude of observational-numerical-synoptic studies has been carried out in relation to the extreme precipitation events over the eastern Mediterranean region to date, such as extreme rainfall analysis (e.g. Alpert *et al.,* 2002; Ben David-Novak *et al.,* 2004; Kostopoulou and Jones, 2005; Ben-Zvi, 2009; Mathbout *et al.,* 2018), trends in extreme precipitation (e.g. Yosef *et al.,* 2009; Shohami *et al.,* 2011; Ziv *et al.,* 2013; Ajjur and Riffi, 2020), satellite remote-sensing-based analysis of precipitation extremes (e.g. Gabella *et al.,* 2006; Mehta and Yang, 2008; Nastos *et al.,* 2013; Yucel and Onen, 2014), numerical modelling and climate change projections of heavy precipitations (e.g. Tous *et al.,* 2015; Romera *et al.,* 2016; Toros *et al.,* 2018; Zoccatelli *et al.,* 2020; Zittis *et al.,* 2020), flash floods and water resources attributed to extreme rainfall events (e.g. Morin *et al.,* 2007; Samuels *et al.,* 2009; Koutroulis and Tsanis, 2010; Tarolli *et al.,* 2012; Varlas *et al.,* 2018; Zoccatelli *et al.,* 2019; Spyrou *et al.,* 2020; Rinat *et al.,* 2021), synoptic analysis of precipitation extremes and floods (e.g. Dayan *et al.,* 2001, 2015; Kahana *et al.,* 2002; Alpert *et al.,* 2004; Tsvieli and Zangvil, 2005; Peleg and Morin, 2012; Raveh-Rubin and Wernli, 2015; Toreti *et al.,* 2016), and cyclogenesis and cyclone tracking (e.g. Alpert and Ziv, 1989; Alpert and Shay-El, 1994; Flocas *et al.,* 2010; Flaounas *et al.,* 2014a, 2014b; Almazroui *et al.,* 2014; Zappa *et al.,* 2014; Ziv *et al.,* 2015).
However, literature review of the Sinai region reveals that very limited studies have been carried out so far mainly on the flash floods associated with heavy rainfall events from the ground/satellite-based data analysis approach (e.g. Roushdi et al., 2016; Dadamouny and Schnittler, 2016; Arnous and Omar, 2018; Morsy *et al.,* 2019; Baldi *et al.,* 2020) to numerical model experiments (e.g. Cools et al., 2012; El Afandi *et al.,* 2013; Morad, 2016; Prama *et al.,* 2020; Omran, 2020; El-Fakharany and Mansour, 2021). In such circumstances, Mohamed and El-Raey (2019) pointed out that limited numbers of extreme precipitation events with high intensities and short durations that typically result in flash floods allegedly are the only sources of the renewable water-resources in the Sinai Peninsula. Thus, it seems necessary to understand, in the first place, the spatiotemporal distribution of extreme precipitation events across the Sinai, and in the second place, to discover the corresponding synoptic-dynamical mechanisms responsible for the occurrence of such events in the region. To our best of knowledge, no study attempted yet to quantify the extreme precipitation characteristics (e.g. anomalies, frequencies and spatial patterns) associated with the synoptic-regional atmospheric circulation and cyclone tracking over the Sinai Peninsula –and even not over the eastern Mediterranean basin, as described and presented in this study. Therefore, to bridge the above-mentioned research-gaps existinng in the Sinai, in this study we address the following main research questions:

i. how are the extreme precipitation climatologies spatiotemporally distributed across the Sinai Peninsula?
ii. which synoptic large-scale systems are responsible for the occurrence of the Sinai's (extreme) precipitation events?
iii. what are the major tracks of cyclones and their frequencies over the region?

In this research, our data-analysis spans the period from 1st of January 2001 to 31st of December 2020. First, we use satellite remote-sensing precipitation to quantify the anomaly, monthly regime, frequency and spatial patterns of the extreme precipitation events, together with the computation of a set of extreme climate indices. Then, the dominant synoptic atmospheric circulation patterns corresponding to the Sinai extreme precipitation events in the wet –and dry periods are explored using reanalysis data at multiple levels of the atmosphere. Finally, a daily-based frequency of the rainfall producing-systems (cyclone tracking) are tracked and plotted over the region for the wet –and dry periods separately.

2 Data and methods

2.1 The description of study area

The Sinai Peninsula is located in the northeast of Egypt with an area of 61,000 km^2 (Fig. 1) covering about 6% of Egypt's area (Mohamed *et al.,* 2014; Badreldin and Goossens 2013). Sinai lies in an arid to hyper-arid belt of North Africa and belongs to the Saharan-Mediterranean climate classification (Dadamouny and Schnittler, 2016). Nevertheless, it is one of the coldest regions in Egypt due to its high altitudes and mountainous topography, where highest elevations are found toward the southern parts (e.g. Mount Catherine, the highest mountain in Egypt with an elevation of 2642 above ground level (AGL), see Fig. 1). Overall, the Sinai region is characterized by a Mediterranean climate in the north and a semidesert/desert climate in the south (El-Sayed and Habib, 2008).

https://doi.org/10.5194/esd-2022-10
Preprint. Discussion started: 25 March 2022

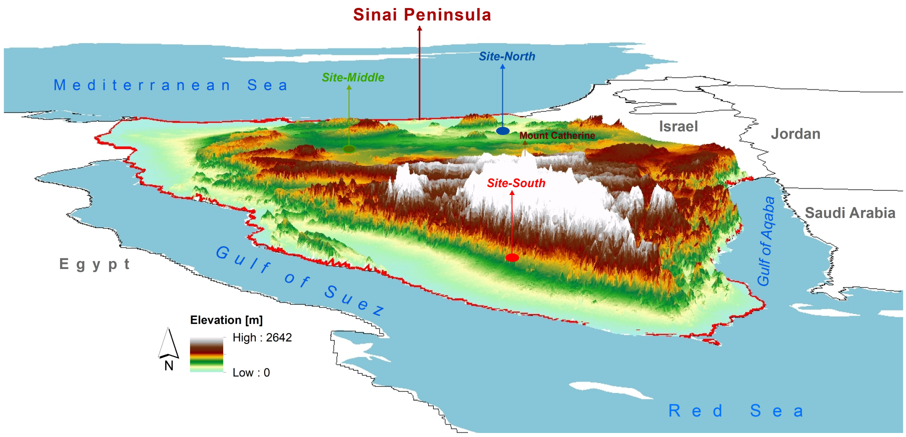

Figure 1. The location of the Sinai Peninsula in northeast of Egypt with the underling three-dimensional topography. Three selected sites in north (Site-North: 30°07'N, 33°09'E), middle (Site-Middle: 30°01'N, 33°50'E) and south (Site-South: 28°50'N, 33°70'E) of the Sinai shown here, used for the site-scale-based calculation of precipitation anomalies.

2.2 Datasets

2.2.1 Satellite Global Precipitation Measurement (GPM)

The Global Precipitation Measurement (GPM) is an international satellite mission to provide quasi-global precipitation estimates with a high temporal resolution (30min, daily and monthly) and spatial resolution (0.1°) through the Integrated Multi-satellitE Retrievals (IMERG) product. The GPM mission follows the Tropical Rainfall Measuring Mission (TRMM) program, aiming at improving the satellite-based precipitation observation capability. GPM-IMERG provides different rainfall estimates that are combined from active and passive instruments in the GPM constellation (https://gpm.nasa.gov/). Further detailed are given by Huffman *et al.,* (2014). The GPM data has been employed in several studies over the Mediterranean region (e.g. Retalis *et al.,* 2018; Petracca *et al.,* 2018; Caracciolo *et al.,* 2018; Cinzia Marra *et al.,* 2019; Hourngir *et al.,* 2021). In this study, we used the IMERG version 6 GPM-Level 3 final precipitation product (30min/daily) to estimate the extreme precipitation characteristics including rainfall anomalies for the selected sites (see Fig. 1 for the locations), monthly precipitation regime, climate indices (see Table 1), and spatiotemporal variations of the extreme precipitation events for a 20-year period (2001-2020) over the Sinai Peninsula.

2.2.2 NCEP/NCAR reanalysis data

To investigate the synoptic-dynamics climatology of the wet-period (October-March) and dry-period (April-September) over the Sinai Peninsula, the required reanalysis variables were obtained from the National Centers for Environmental Prediction and National Center for Atmospheric Research (NCEP/NCAR) https://psl.noaa.gov/data/gridded/data.ncep.reanalysis.html. NCEP/NCAR provides the reanalysis data with 6-hours, daily and monthly time-steps at the surface and multiple levels of the atmosphere since 1948 onward with a global 2.5° × 2.5° grid (Kalnay 1996). These datasets have been used in the Mediterranean region in several studies especially with regard to the synoptic analysis of precipitation, blocking systems, storm and cyclone tracking (e.g. Krichak *et al.,* 2002; Trigo *et al.,* 2004; Tolika *et al.,* 2006; Trigo, 2006; Lois, 2009; Barkhordarian *et al.,* 2013; Almazroui and Awad, 2016; Almazroui *et al.,* 2014, 2017; Kotsias *et al.,* 2020). In this study, we used the NCEP/NCAR reanalysis data, among others e.g. ERA-Int with 1.125° spatial grid, due to its coarser resolution. This is mainly because large-scale synoptic systems such as cyclones and anticyclones can be more clearly represented in a coarse resolution; whereas, those will be splitted up into many small-scale systems in the finer resolutions making it hard to diagnose the main controlling patterns. The following NCEP/NCAR reanalysis daily meteorological variables -or derived parameters at multiple atmospheric levels were employed: sea level pressure

https://doi.org/10.5194/esd-2022-10
Preprint. Discussion started: 25 March 2022

SLP (hPa), geopotential height HGT (m), relative vorticity RV (10^{-5} S^{-1}), zonal (U) and meridional (V) wind-components (m s^{-1}), and vertical velocity (omega: Pa s^{-1}).

2.3 Data analysis approach

2.3.1 Calculation of the precipitation anomalies

The annual and seasonal changes in total precipitation trend were estimated using the satellite GPM-based daily precipitation over the period of 2001-2020 for the three selected sites across the Sinai (see Fig. 1 for the locations). The climatology mean precipitation values and spatial distribution were the main criteria for the selection of the sites. In this way, each chosen site is representative for its surrounding area in terms of both the precipitation magnitude and spatial patterns. Thus, the selected sites in north, south and middle parts indicate the max, min and average amounts of precipitation received across the Sinai region, respectively over a 20-year time-period (see Fig. 4a). For this analysis, precipitation anomalies (annual and seasonal) are calculated in three steps: i) calculating the climatology mean of the data, ii) subtracting the mean value from the each year/season values, and ii) drawing the trend of slopes using the least squares method. Here, the winter includes DJF months (Dec, Jan, Feb) and the autumn includes SON months (Sep, Oct, Nov). Precipitation anomalies for the spring and summer periods were found to be close to zero, and therefore excluded.

2.3.2 Estimate of the extreme precipitation indices

The spatiotemporal analysis on the satellite GPM-based daily precipitation timeseries was carried out for the entire Sinai region. For this, a set of climate functions/indices (see Table 1 for the details) was computed for the period of 2001-2020 using the Climate Data Operator (CDO) (Schulzweida, 2020), developed in Max-Planck-Institute for Meteorology (https://code.mpimet.mpg.de/projects/cdo).

Table 1. CDO functions and climate indices used in this study (Schulzweida, 2020).

Index	Descriptive name	Definition	Units
monsum	Monthly sum	For every adjacent sequence $t\_1, ..., t\_n$ of time steps of the same month it is: $o(t, x) = \text{sum}\{i(t', x), t_1 < t' \leq t_n\}$	mm
yearsum	Yearly sum	For every adjacent sequence $t\_1, ..., t\_n$ of time steps of the same year it is: $o(t, x) = \text{sum}\{i(t', x), t_1 < t' \leq t_n\}$	mm
eca_pd	Precipitation days index per time period	Generic ECA operator with daily precipitation sum ≥5 mm.	days
eca_r10mm	Heavy precipitation days index per time period	Specific ECA operator with daily precipitation sum ≥10 mm	days
eca_r20mm	Very heavy precipitation days index per time period	Specific ECA operator with daily precipitation sum ≥20 mm	days
eca_cdd	Consecutive dry days index per time period	Maximum number of dry days with daily precipitation sum ≥1 mm	days
eca_rr1	Wet days index per time period	Number of wet days with daily precipitation sum ≥1 mm	days
eca_sdii	Simple daily intensity index per time period	Average precipitation on wet days with daily precipitation sum ≥1 mm	mm/day

2.3.3 Synoptic analysis

To explore the synoptic and dynamics climatologies at multiple level of the atmosphere responsible for the occurrence of the extreme precipitation events over the Sinai, the daily reanalysis data obtained from NCEP/NCAR was investigated. In the first place, the wet-period and dry-period were splitted using the extreme precipitation indices described above. We realized that, a threshold of ≥10 mm/day is desirable in determining the wet and dry periods for the Sinai region. Thus, the wettest months were found from October to March, defined as the wet-period, and the driest months from April to September, defined as the dry period. In the second place, using the

https://doi.org/10.5194/esd-2022-10
Preprint. Discussion started: 25 March 2022

above-mentioned satellite-reanalysis variables (see Sect. 2.2.), the dominant synoptic features and regional atmospheric circulation patterns accompanied by the spatial correlations between the Sinai's precipitation and key meteorological variables were computed and analyzed for the wet and dry periods for the climatology period of 2001-2020.

2.3.4 Cyclone tracking

In line with the synoptic analysis mentioned above, the daily trajectories of the rainy systems (cyclones) precipitated over the Sinai region (≥10mm) were tracked and plotted for the wet and dry periods (2001-2020). This analysis consists of three major steps as follows: First, daily composites of SLP together with the relative vorticity and streamflow at 850-hPa level were generated i.e. 7305 composites maps at a synoptic-scale; and the same numbers of daily total precipitation maps were produced over the Sinai Peninsula also. Second, all the 20-year daily precipitation events of the Sinai were monitored one-by-one, those with <10mm disregarded, and the remaining events were classified into five categories based on rainfall magnitude as follows: category 1 (10-20mm), category 2 (21-30mm), category 3 (31-40mm), category 4 (41-50mm) and category 5 (>51mm). For each classified rainfall-event the corresponding cyclone was tracked since it was born (cyclogenesis) until disappeared (cyclolysis) from the region using the above-mentioned composite charts. Third, finally the cyclone tracking charts for the wet and dry periods produced over the study area.

3 Results

3.1 Climatology analysis of the precipitation characteristics

3.1.1 Annual and seasonal changes in precipitation trend

The average changes in the annual and seasonal precipitation trends during the recent period of 2001-2020 across the Sinai Peninsula are shown in Fig. 2. The sign and magnitude of both annual and seasonal precipitation variations do not show spatial continuity Sinai-wide, rather indicating a spatially dependency. This implies that, the site located in north of the Sinai (Fig. 2a, see Fig. 1 for the location) exhibits a greater rate of the annual and interannual changes with a higher anomaly (approx. ±45 mm/decade) compared to the sites located in the middle (Fig. 2b) and south (Fig. 2c) of the Sinai. The largest annual (inconsiderable) negative trend is found in north of the Sinai (−0.03 mm/decade), while the central (0.10 mm/decade) and southern (0.36 mm/decade) sites exhibit positive trends. This means that, annual precipitation rates over the northeastern parts and middle-towards-southern parts of the Sinai are experiencing a drier and wetter climatic condition, respectively. In terms of interannual trends, all sites show positive changes, expect for the winter precipitation in the north-site expressing a remarkable negative trend (-1.11 mm/decade), as shown in Fig. 2a. Amongst, the maximum and minimum positive interannual changes are found in wintertime precipitations of the south-site (0.55 mm/decade) and the middle-site (0.03 mm/decade), respectively (Figs. 2b and 2c).

https://doi.org/10.5194/esd-2022-10
Preprint. Discussion started: 25 March 2022

Earth System Dynamics
Discussions

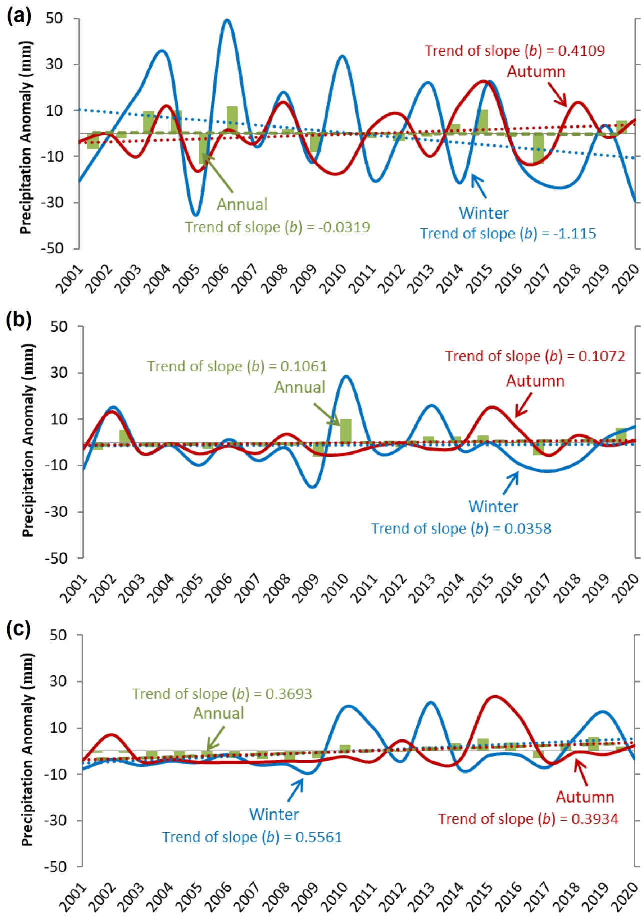

Figure 2. Annual and seasonal changes in the total precipitation (mm) for three selected sites in (a) north, (b) middle and (c) south of the Sinai Peninsula during 2001-2020. For the locations of the sites, see Figure 1. In the panels, winter (DJF) in given in blue, autumn (SON) is given in red, and annual in green color.

3.1.2 Precipitation regime

Figure 3 represents the monthly precipitation regime climatologies (2001-2020) over the Sinai region. High (>20%) ratios of monthly precipitation over annual precipitation are estimated in the winter months of January and February, mostly found in the mid-to-north of the Sinai. March indicates some patches of high ratios in the south and northwest also, as shown in Fig. 3a. However, the period of April to September (colored in black in the legend) receives less than 20% ratio of the annual precipitation. This implies that spring and summer months experience longer dry weather periods than the winter season. Considering the autumn months, the areas with 20% ratio of annual precipitation remain largely out of the Sinai domain, expect for a few mini-patches. Therefore, winter is the rainiest season throughout the Sinai. It is also noted that, full ratios of monthly precipitation to annual precipitation for individual months of the year are illustrated in Fig. S1, which provides further details on the monthly precipitation regime in the study area. Furthermore, to compare the monthly ratios of precipitation across the Sinai, the bar charts for the given sites covering the whole Sinai were plotted (Figs. 3b-3g). The highest and lowest ratios are found in the winter and summer months, respectively. However, by a closer look it becomes clear that chosen sites do vary in terms of magnitude and trends in the monthly precipitation ratios. For instance, in most sites the highest monthly ratio is observed in February, except for sites located in the Sinai southwest (which, is January – Fig.3d) and southeast (which, is March - Fig.3g). Likewise, an inconsistent seasonal trend is also

https://doi.org/10.5194/esd-2022-10
Preprint. Discussion started: 25 March 2022

Earth System Dynamics
Discussions
Open Access

remarkable for the autumn months, meaning that the northern sites indicate an positive trend from late summer to the end of autumn (Figs. 3a, 3b and 3e). The southern sites, however, represent a contrasting pattern with respect to the monthly precipitation regime (Figs. 3d, 3f and 3g).

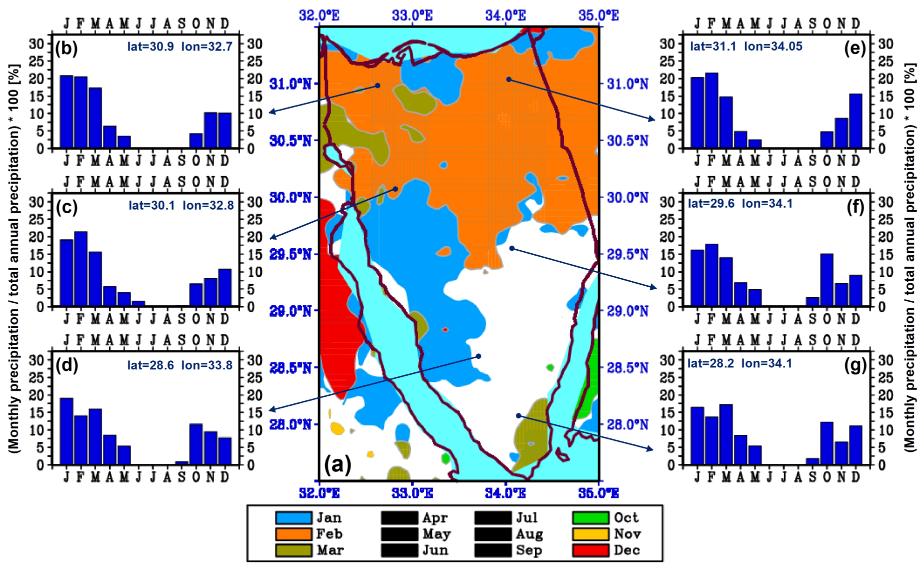

Figure 3. Monthly precipitation regime: (a) ratio of monthly sum precipitation to annual total precipitation (%), where only ratios >20% are plotted for each month; panels b-g indicate the monthly ratios (January to December) for the selected sites across the Sinai Peninsula for the climatology period of 2001-2020. It is noted that in the panel a, the monthly ratios from April to September (colored in black in the legend) are below 20%, thus not ploted here, but full ratios (%) are illustrated in Fig. S1 in a monthly basis.

3.1.3 Spatiotemporal variations of the extreme precipitation events

The spatial precipitation patterns in terms of the climatology average, the rainiest month and the wettest day for the period of 2001-2020 in the Sinai Peninsula are illustrated in Figure 4. The climatology map of precipitation markedly demonstrate that northeast and southwest parts of the Sinai receive the highest (ranged between 100 and 150 mm/year) and the lowest (ranged between 20 and 30 mm/year) amounts of annual precipitation, respectively (Fig. 4a). This implies that precipitation unevenly distributed over the Sinai. However, most parts of the region receive not as high as 40 mm/year, except for the northern areas close to the Mediterranean Sea. With respect to the occurrence of the precipitation extremes in the Sinai, we discovered that the rainiest month (out of 240 months) was in March 2020 (Fig. 4b) with a wide range of rainfall values from 15 to 30 mm/month in the south and from 50 to 70 mm/month in the north. Interestingly, the wettest day (out of 7305 days) has been occurred in the same month/year, that is March 12, 2020 (Fig. 4c), thus it is not surprising to see an analogous spatial pattern when compared to the rainiest month (Fig. 4b) but with less magnitude.
We also identified the twelve rainiest months out of 240 months (see Fig. S2) and the twelve wettest days out of 7305 days (see Fig. S3). It was found that 9 out of 12 extreme month/day cases occurred in the winter season (Jan, Feb and Mar) with the highest frequency occurrence in January (5 cases); while only 3 out of 12 cases took place in autumn (Oct and Dec). In all the extreme precipitation cases, either the rainiest months –or the wettest days, a similar spatial pattern was captured with respect to the spatial precipitation distribution, meaning that the maxima were recorded in the north and the minima in south of the Sinai Peninsula.

https://doi.org/10.5194/esd-2022-10
Preprint. Discussion started: 25 March 2022

Earth System Dynamics
Discussions

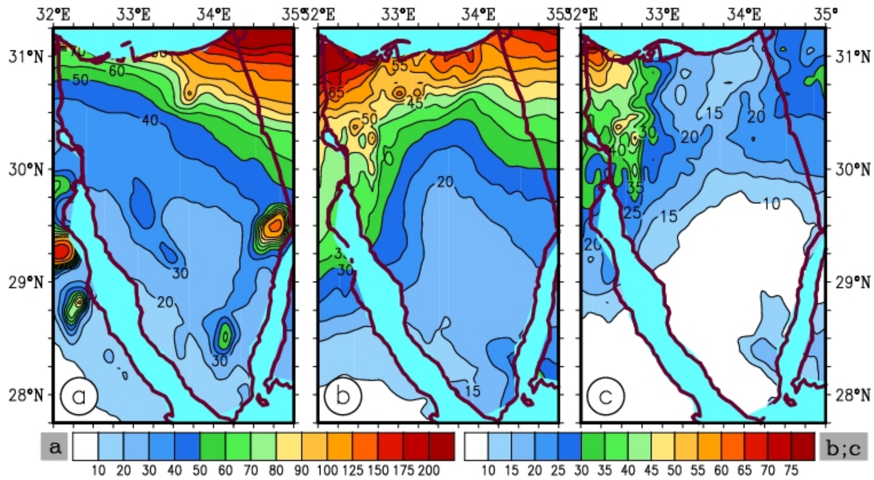

Figure 4. The precipitation spatial patterns over the Sinai Peninsula: a) climatology map of mean annual precipitation (2001-2020); b) the wettest month i.e. March 2020 (out of 240 months); and c) the wettest day i.e. March 12, 2020 (out of 7305 days). Units are in mm.

With respect to abundance of extreme rainfall events, frequency occurrence of the Sinai's precipitation extremes with different thresholds was plotted (see Fig. S4). The highest and lowest frequencies with a threshold of ≥5 mm/day are occurred in the north (ranged between 100 and 250) and south of the Sinai (ranged between 20 and 40), respectively. Higher precipitation frequency thresholds of ≥10 mm/day and ≥20 mm/day follow the same spatial pattern as to threshold of ≥5 mm/day across the region, but with much lower frequencies. The distribution of the extreme precipitation frequencies, regardless of their thresholds, are in very good agreement with the spatial pattern of the precipitation climatology map (see Fig. 4a).

To find out the precipitation spatial patterns of the Sinai at monthly basis, the frequency of events with ≥10 mm/day, as a middle-threshold among others, was selected. According to Figure 5, the occurrence of the precipitation frequencies with ≥10 mm/day are limited to the cold periods of winter (ranging from 1 to 40, Figs. 5a-5c) and autumn (ranging from 1 to 30, Figs. 5j-5l). While for the period from April to September (the growing season) almost no precipitation has been recorded (Figs. 5d-5i), suggesting a prolonged dry-period in the region. The winter months comparatively receive higher numbers of rainfall events especially in the northeast (with the maximum frequencies in January (Fig. 5a)), when compared to the autumn months (with the minimum frequencies in November (Fig. 5k)). It is worth mentioning that, monthly spatial precipitation patterns with a threshold frequency of ≥ 20 mm/day were computed also (see Fig. S5). It was found that the frequency occurrence of the extreme events reduced almost by half in comparison with ≥10 mm/day precipitation frequency (Fig. 5). Furthermore, it is mostly occurred in the late autumn and early winter episodes, and only limited to a small part of the northeastern Sinai.

https://doi.org/10.5194/esd-2022-10
Preprint. Discussion started: 25 March 2022

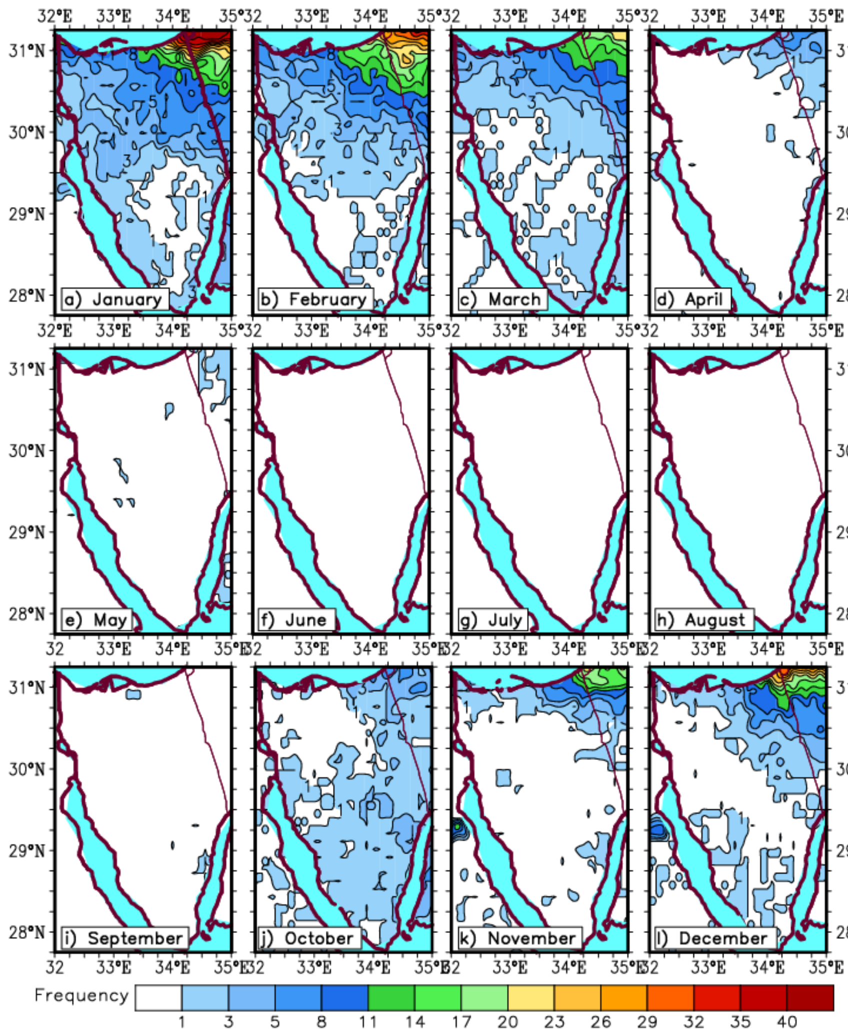

Figure 5. Frequency occurrence of the monthly precipitation climatology events with a threshold of ≥10 mm/day for the period of 2001-2020 (7305 days) over the Sinai Peninsula. Units are in days.

The dryness and wetness conditions across the Sinai region were also explored by computing the simple daily intensity index (SDII), number of consecutive dry days (CDD) and number of wet days (RR1) (Fig. 6). It can be clearly seen that the highest SDII is observed in the northeast with an intensity of ≥6 mm/day. Interestingly, the lowest SDII is not seen in the south (even though the minimum precipitation magnitude and frequency is located there – see Fig. 4), but in central parts of the Sinai with ≤3 mm/day (Fig. 6a). CDD is remarkable in the south with ≥600 out of 7305 days, indicating that these areas receive less than 1mm rainfall for a long period; however, it is gradually decreasing northward with ≤300 days (Fig. 6b). Unlike CDD, it is not surprising to observe that RR1 is the lowest in the south (≤100 days) and innermost parts (≤200 days), but rapidly increases towards the northeast of the region (≥350 days), as shown in Figure 6c. These results (Fig. 6) are in good agreement with the above findings over the Sinai Peninsula.

https://doi.org/10.5194/esd-2022-10
Preprint. Discussion started: 25 March 2022

Earth System Dynamics
Discussions

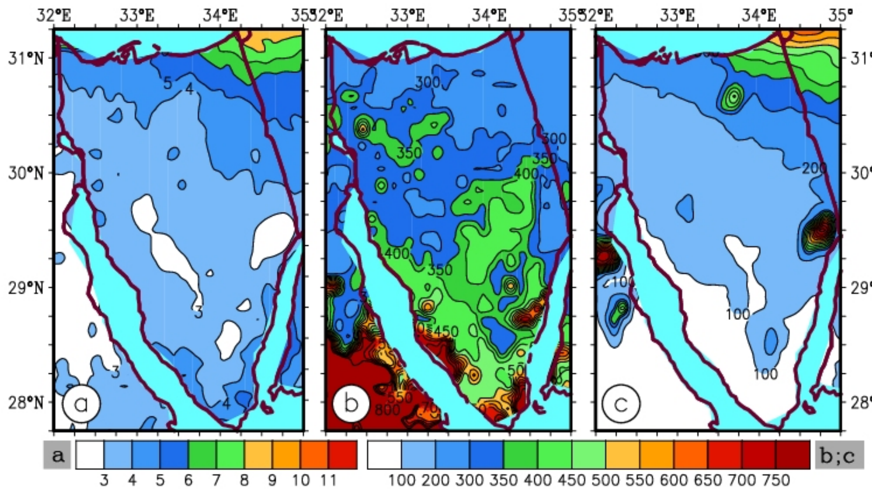

Figure 6. The extreme daily precipitation indices with a threshold of ≥1mm/day: a) simple daily intensity index (SDII, *mm/day*), b) consecutive dry days (CDD, *days*), and c) wet days index (RR1, *days*) for the period of 2001-2020 (7305 days) over the Sinai Peninsula. Units are: (a) in mm and (b-c) in days.

Lastly, we plotted the monthly precipitation climatologies (2001-2020) together with ranks of 12 months (out of 240) with the highest amount of precipitation received in the Sinai Peninsula (Fig. S6a). The most extreme precipitation event occurred in March 2020 over the past two decades, followed by February 2019 and January 2013. Also, timeseries of areal-averaged daily precipitation in the year 2020 was illustrated over the Sinai (Fig. S6b). The precipitation distribution is noticeably limited to the cold months (October-March), which is consistent with Figure 5, with the severest storm recorded during 11-13 March (Fig. S6c). Allegedly, the peak rainfall hours (>30mm) occurred in the afternoon of the March 12, 2020, as represented by onset and termination of the most powerful rainy system in hourly intervals of the subplot in Fig. S6c. It may worth mentioning that, the exceptional storm event of 11-13 March 2020 over the Sinai is deeply investigated via a data-analysis and simulation-experiment approach in a follow-up research.

3.2 Synoptic analysis of the wet and dry periods

Spatial distribution of the monthly mean precipitation amounts and magnitudes indicated a remarkable difference between the wet period (ranged 5-70 mm/month) and dry period (ranged 1-3 mm/month) for the climatology period of 2001-2020 over the Sinai Peninsula (see Fig. S7). However, despite a large dissimilarity in precipitation values of the wet and dry periods, their spatial pattern climatologies largely resemble. This implies, precipitation amounts in both periods are notably increased from southern parts towards northeast of the Sinai. In the follow-up sub-sections, therefore, the atmospheric large-scale systems corresponding for the occurrence of the wet and dry periods are synoptically investigated.

3.2.1 Synoptic patterns and atmospheric circulation structure

Figure 7 represents the climatology (2001-2020) of the synoptic patterns and cyclogenesis at suface and 500-hPa atmospheric levels during the wet and dry periods over the Mediterranean basin including the Sinai Peninsula (marked by a red box). In the wet period at surface level (Fig. 7a), two major sources of strong cyclonic activities (cyclogenesis) are observed over the Mediterranean westen part (at the lee of Alps Mountains over Gulf of Genoa) and eastern part (at the lee of Taurus Mountains over Cyprus) – see Fig. 12 for the locations. These areas are found by the closed SLP contours along with strong positive vorticity over the west and east parts of the Mediterranean Sea, respectively. Cyprus low alegedly is responsible for the occurrane of majority of rainfall events over the eastern Mediterranean including the Sinai. For instance, about 80% of the rainfall in the cold period of Israel are associated with the Cyprus cyclone systems, as pointed out by Saaroni *et al.,* (2010). In wet period, the Red Sea

https://doi.org/10.5194/esd-2022-10
Preprint. Discussion started: 25 March 2022

Earth System Dynamics
Discussions
Open Access

trough as a lower-level system, is another significant synoptic system that influencing the eastern Mediterranean region, but mostly in the autumn (Ziv *et al.,* 2021). As shown in Fig. 7a, this trough is developed as a result of the coexistence of the eastern African cyclone namely Sudan's Low and Saudi Arabia's anticyclone. Its high impact on the eastern Mediterranean area is depending on the position of the Red Sea trough axis, that is, the eastern position, as pointed out by e.g. Saaroni *et al.* (1998), and Tsvieli and Zangvil, (2005). However, the impact of the Red Sea trough on the Sinai's rainfalls is limited compared to northeastern parts of the Mediterranean basin, mostly due to the geographical location of the Sinai. In line with the lower levels, the pressure pattern at 500-hPa level shows a synoptic-scale trough (of the persistent low center) with high positive vorticities providing a suitable condition for occurrence of rainfall events over the Mediterranean region extending towards the Middle-East areas (Fig. 7b).

In contarst to the wet period, surface level pattern of the dry period differs strongly over the region (Fig. 7c). In the dry period, hardly ever cyclones are produced in the western Mediterranean as dominated by the high-pressure systems extending from the north Atlantic Ocean and north of Africa. Limited low-pressure systems however are typically developed over the eastern Mediterranean. This is due to the formation of a trough extending from the Persian Gulf (which, developes as the result of the topographic impact of Zagros Mountains in western Iran) via Taurus Mountains in the southern Turkey into the eastern Mediterranean basin (see Fig. 12 for the locations). The Sinai region locating in the southeastern Mediterranean basin, as shown in Fig. 7c, is highly influenced by the ridge of the north Africa so-called Azores anticyclone, rather than the Persian Trough that impacting mostly the northeastern parts of the Mediterranean. Thus, at midlevel of 500-hPa geopotential height, the eastern Mediterranean is mostly subjected to persistent air subsidence, and only a limited trough is formed with relatively high positive vorticity over the eastern Mediterranean (Fig. 7d). This results in preventing rainfall to a large extent over the region during the dry period. Therefore, the Sinai area recieves much less amount of precipitation in terms of magnitude and frequency, compared to those received over northeastern parts (such as Israel) of the Mediterranean basin. These results are in good agreement with the findings reported by Alpert *et al.* (1990) and Saaroni and Ziv (2000).

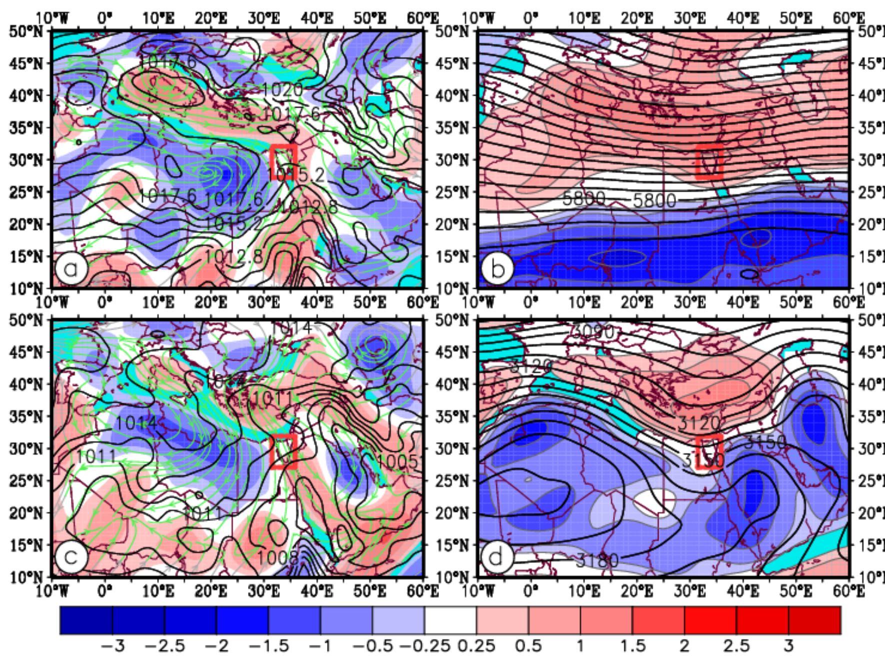

Figure 7. Climatology synoptic condition during the wet-period from October to March (a and b) and dry-period from April to September (c and d) during the period of 2001-2020 over the Sinai Peninsula (red box in each panel);

https://doi.org/10.5194/esd-2022-10
Preprint. Discussion started: 25 March 2022

Earth System Dynamics Discussions

a) composites of sea level pressure (*black contours*, hPa), 925-hPa relative vorticity (*shading*, 10^{-5} S^{-1}) and streamflow (green streamline); b) 500-hPa composite of geopotential height (*isolines,* m) and relative vorticity (*shading,* 10^{-5} S^{-1}); c and d same as in ***a*** and *b* panels respectively, but for the dry period.

Besides the synoptic pressure-systems described above, veritical velocity motions (omega) could further reveal discrepancies between the wet and dry periods, from a dynamical perspective. Increase in the synoptic precipitatin events over the wet period is inevitably attributed to the existance and duration of strong rising parcls of air and upward vertical streams over the Sinai -and in the nearby regions. The omega cross-section along the longitude (Fig. 8a) represents a maximum core with negative value of -0.03 Pa s^{-1} occurs at 800-700 hPa levels (at above 36°E) extending up to 250 hPa. It also indicates that, unlike to the western parts, eastern parts of the Sinai experiencing a relatively strong rising condition at multiple levels of the atmosphere during the wet period.

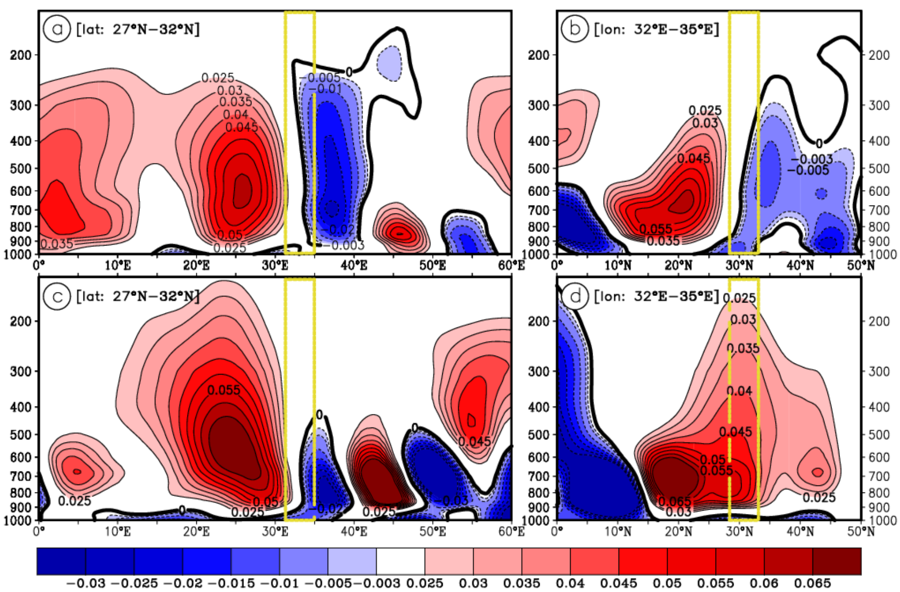

Figure 8. Vertical velocity cross-section (omega: Pa s^{-1}) for: the wet period of October to March (a and b), and dry period of April to September (c and d) over the period of 2001-2020. Omega values averaged for the latitudes of 27°N-32°N across the longitude (a and c panels), and for the longitudes of 32°E-35°E across the latitude (b and d panels). Yellow box in each panel indicates the location of Sinai Peninsula along longitude and latitude.

A similar pattern analogous to the longitude cross-section is observed also along the latitude (Fig. 8b). This means that, the maximum core of vertical velocity with the value of -0.006 Pa s^{-1} is seen towards the northeast of the Siani (at below 35°N) in particular at higher levels. However, when it comes to the dry period, a much weaker negative omega is observed, mostly limited to lower levels of the atmosphere along the longitude (Fig. 8c), and it is alegedly positive (sinking) in particular on the southern parts of the Sinia region along the latitude (Fig. 8d). In such circumstances, the rising of air is strictly restricted. These results (Fig. 8) therefore further clarify, among many others, why the northeast-parts of the Sinai receive higher (intense) amount of precipitation compared to rest of the Sinai Peninsula, that is, partially due to the stronger vertical velocity motions in both the dry –and especially wet periods.

https://doi.org/10.5194/esd-2022-10
Preprint. Discussion started: 25 March 2022

Earth System Dynamics Discussions

3.2.2 Spatial correlation analysis

In this section, daily-scale relationships of the Sinai's rainfalls associated with the regional atmospheric variations responsible for the occurrence of wet and dry periods are explored. Figures 9a and 9b show the spatial correlation patterns between the Sinai's precipitation and regional see level pressure (SLP) during the wet-period and dry-period, respectively. A meaningful negative correlation (r = -0.1) is seen over the Sinai region. This indicates that a strong association is realized between higher rainfall events (magnitude and frequency) and lower surface pressure fields over eastern Mediterranean including the Sinai in wet period (Fig. 9a). Contrariwise, a positive correlation (r = 0.25) is found between the rainfall and SLP over the Sinai (Fig. 9b), highlighting the dominance of high-pressure fields over the region that restrict rising of the air during the dry period. The spatial patterns at midlevel of 700-hPa also represent a meaningful negative correlation (r = -0.24) between the Sinai's rainfall and geopotential height (HGT) during wet period (Fig. 9c). A similar spatial pattern with a higher correlation coefficient (r = -0.3) is observed in the dry period also. However, a significant decrease in the region's precipitation could be justified by the predominance of subtropical high-pressure centers and increase of HGT during the dry period; thus, a meaningful relationship is formed between the two (Fig. 9d). The potential vorticity (PV) at the low-level of 1000-hPa correlates positively with the rainfalls in both wet and dry periods, indicating a cyclonic circulation in lower atmosphere over the Sinai region. However, positive PV (r = 0.12) has been dominated over the eastern Mediterranean including the Sinai during the wet period (Fig. 9e); whereas, its impact remarkably diminished over the region in dry period (Fig. 9f), resulting in decrease of precipitation in the eastern Mediterranean basin.

https://doi.org/10.5194/esd-2022-10
Preprint. Discussion started: 25 March 2022

Earth System Dynamics
Discussions

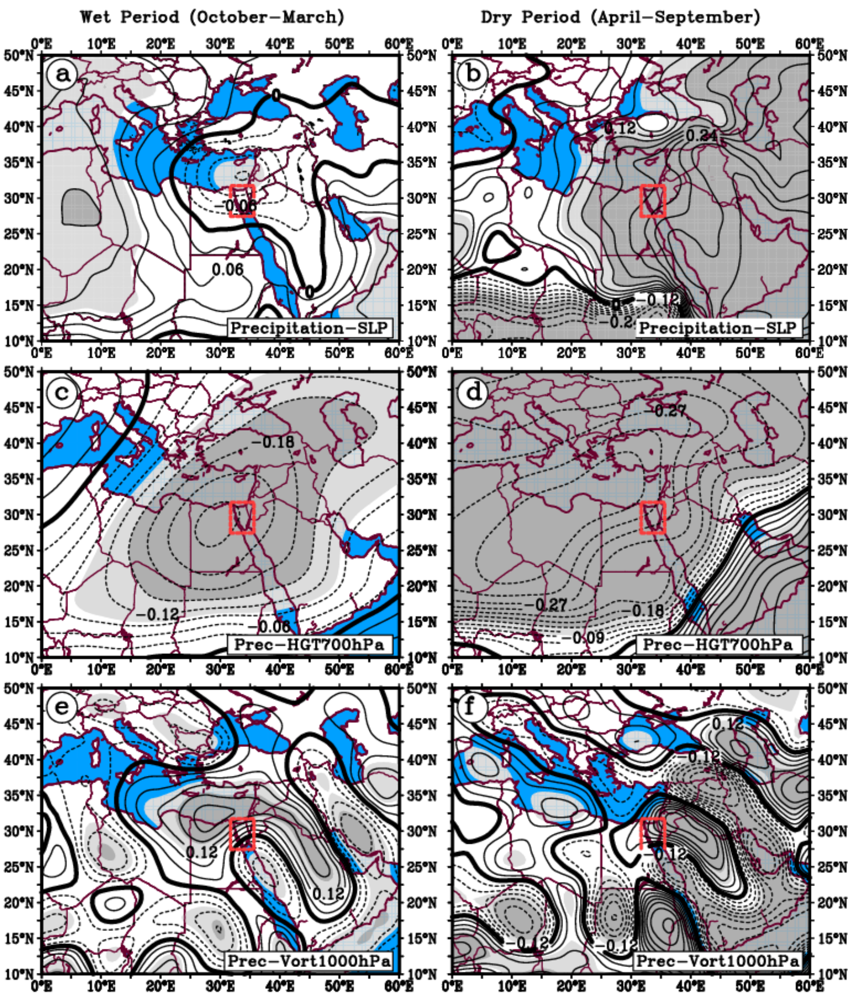

Figure 9. Spatial correlation patterns between the daily precipitation amounts averaged over the Sinai Peninsula (red box in each panels) and key atmospheric variables for the wet-period of October to March (left panels) and dry-period of April to September (right panels) over the period of 2001-2020. In each panels, correlations are between precipitation and: (a and b) SLP; (c and d) geopotential height HGT at 700-hPa; and (e and f) relative vorticity RV at 1000-hPa. The 95% and 99% meaningful correlations are shown in light-gray and dark-gray colors, respectively.

A coupling-correlation-pattern, as shown in Fig. 10, is observed with respect to the precipitation and the meridional wind (V-wind) at 925-hPa level over the Sinai region during the wet period (Fig. 10a). This indicates, the Sinai's rainfall positively correlated (r = 0.12) with southerlies found across the Middle-East with a core on the Mesopotamia, see Fig. 12 for the locations), but negatively correlated (r = -0.15) with northerlies found over central/eastern Mediterranean and north of Africa. This provides a suitable condition for moisture transport from the Red Sea (by the southerlies) and the Mediterranean Sea (by the northerlies) into the study area.

https://doi.org/10.5194/esd-2022-10
Preprint. Discussion started: 25 March 2022

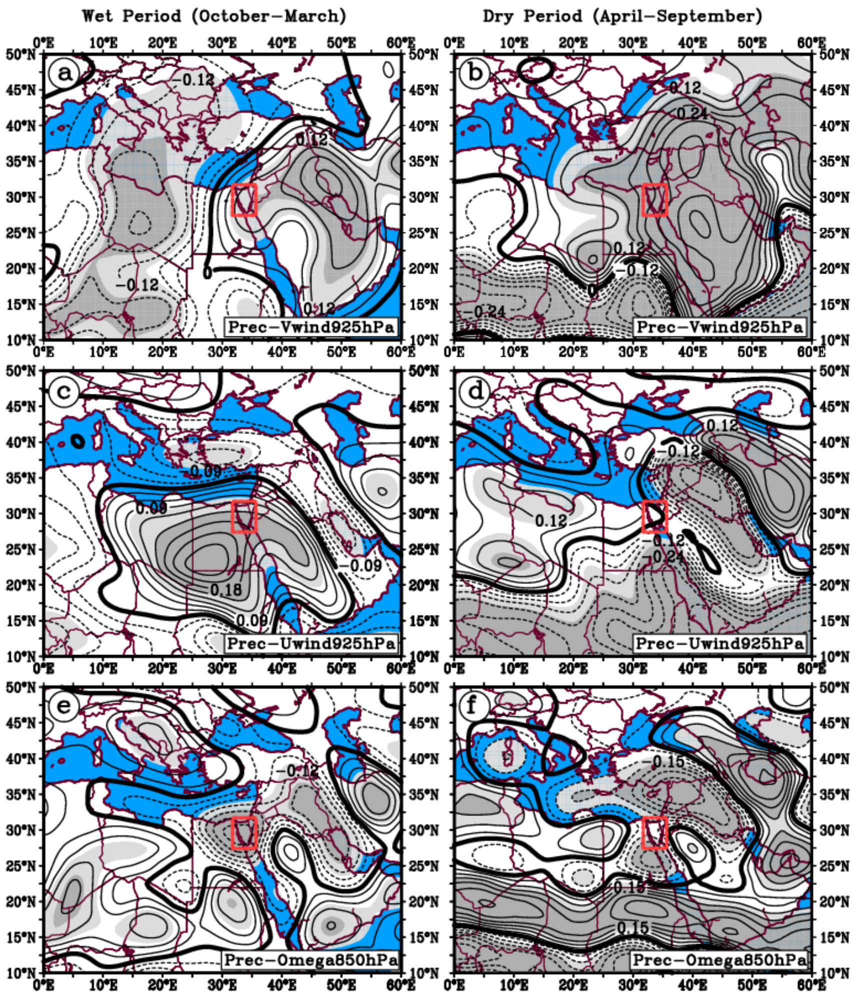

Figure 10. Same as in Fig. 9, but for the correlations between precipitation and: (a and b) meridional wind (V-wind) at 925-hPa; (c and d) zonal wind (U-wind) at 925-hPa; and (e and f) vertical velocity (omega) at 850-hPa.

In contrast, the region is dominated by the southerly winds during the dry period (Fig. 10b), which limits the role of Mediterranean to feed the region with abundant moisture, thus rain events are largely reduced. Interestingly, likewise the V-wind, a similar coupling-pattern is also observed between precipitation and zonal wind (U-wind) at 925-hPa level over the area during wet period (Fig. 10c). In such circumstances, the Sinai's rainfall positively correlates ($r = 0.15$) with westerlies over the eastern Mediterranean basin. However, in the dry period (Fig. 10d), the Sinai's precipitation is largely associated with the negative predominant westerlies over the Mesopotamia and north of Saudi Arabia. Finally, the Sinai's wet period rainfall correlates negatively ($r = -0.18$) with the omega at lower atmosphere (at 850-hPa, Fig. 10e) over the eastern Mediterranean basin indicating a strong vertical velocity. The relationships of the Sinai's rainfall and vertical velocity are largely weakened ($r = -0.08$) during the dry period (Fig. 10f), thus limits the rising of air to a large extent.

https://doi.org/10.5194/esd-2022-10
Preprint. Discussion started: 25 March 2022

Earth System Dynamics
Discussions
Open Access
EGU

3.3 Cyclone tracking in the wet and dry periods

Figure 11 illustrates the daily tracks of cyclones (with a rainfall ≥10mm/day) over the Sinai region in the wet and dry periods for the climatology period of 2001-2020. Total numbers of cyclones during the wet and dry periods were found to be 125 and 31 cases, respectively. The cyclones of each period were classified into five categories (see Table 2) based on the total rainfall received across the Sinai Peninsula. During the wet period, large majority of the cyclone systems (75%) occur within the categories of 1 and 2 (rainfall ranged 10-30mm/day). This implies that less significant storms have struck the Sinai during wet period. Yet, about 15% of the cyclones (with a rainfall >40mm/day) are potentially able to produce torrential rainfalls, which may lead to flash floods over the region.

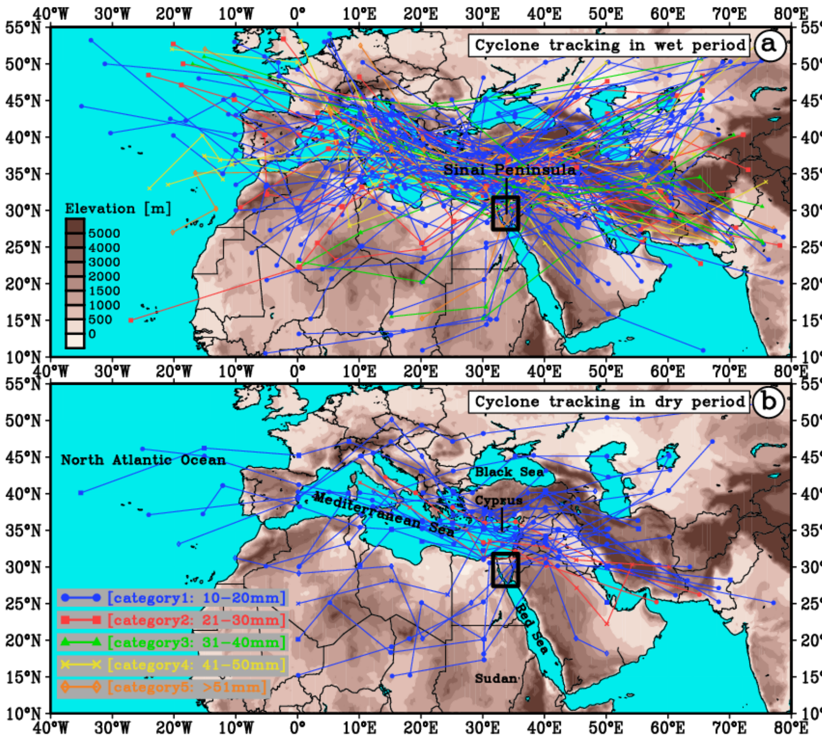

Figure 11. Daily track of cyclones that precipitated (≥10mm/day) over the Sinai Peninsula during: (a) wet-period from October to March, and (b) dry-period from April to September for the climatology period of 2001-2020 (7305 days). Details of all cyclones (156) classified into five categories are given in Table 2.

Table 2. Cyclone tracking characteristics over the Sinai Peninsula for the period of 2001-2020.

Cyclone classification	Total precipitation range	Frequency and percentage of cyclones	
		Wet period	**Dry period**
Category 1	10-20 mm	77 (61.2%)	27 (87%)
Category 2	21-30 mm	17 (13.8%)	4 (13%)
Category 3	31-40 mm	12 (9.7%)	-
Category 4	41- 50 mm	10 (8.1%)	-
Category 5	> 51 mm	9 (7.2%)	-
-	-	125 (100%)	31 (100%)

https://doi.org/10.5194/esd-2022-10
Preprint. Discussion started: 25 March 2022

Concerning the cyclogenesis, the Mediterranean Sea plays a significant role on either cyclogenesis -or strengthening the cyclones passing through the region (Alpert and Shay, 1994; Flocas *et al.,* 2010; Almazroui *et al.,* 2014); this point becomes clear by looking at Fig. 11a. However, considerable numbers of the cyclonic systems are also generated either in the North Atlantic Ocean (then, transferred into the region via passenger cyclones) -or as the result of the Red Sea Trough (Krichak *et al.,* 1997; de Vries *et al.,* 2013; Hochman *et al.,* 2020). Figure 11b also shows the daily tracks of 31 cyclones passed through the Sinai region during the dry period. Unlike to the wet period (Fig. 11a), not only the number of cyclones reduced significantly, but also their magnitudes. The highest frequency of cyclones, according to Table 2, occurs in category 1 with 27 cyclones (87%); and followed by only 4 cyclones (13%) in the category of 2, which have been formed within the Mediterranean (unlike category 2 of the wet period) and then moved eastwards. Interestingly, no cyclonic systems (with a rainfall >10mm/day) taken place within the past twenty-years during the dry period over the Sinai region.

4 Discussion

The main focus of this study remains on quantifying the extreme precipitation events from a statistical and synoptic perspective over the Sinai Peninsual in the eastern Mediterranean basin over the past two-decades. The literature of the Sinai area is poor; meaning that, although several (relavent) studies have been conducted over the eastern Mediterranean (e.g. Krichak *et al.,* 1997; Alpert *et al.,* 2002; Gabella *et al.,* 2006; Nastos *et al.,* 2013; Mathbout *et al.,* 2018; Rinat *et al.,* 2021); minimal studies however are available over the area, yet mostly focused on heavy rainfall-related flash floods (El Afandi *et al.,* 2013; Dadamouny and Schnittler, 2016; Arnous and Omar, 2018; Baldi *et al.,* 2020; El-Fakharany and Mansour, 2021). Thus, the novelty of this research is a combination of the satellite-reanalysis approach for a long-term data analysis. This enabled us to quantify precipitation characteristics (i.e. annual/inter-annual anomalies, monthly regime, magnitude, frequency and spatial patterns), and to discover the major synoptic systems (cyclogenesis, regional circulation pattern, spatial correlation and cyclone tracking) attributed to the occurrence of such heavy rainfalls across the Sinai region.

Our statistical analysis, as one of the first analyses over the Sinai, revealed that distribution of the rainfall events significantly varies in time and space over the region. Temporally, the annual and interannual precipitation trends showed mostly positive tendencies in most parts, especially towards south of the area (Fig. 2). This result is consistent with the previous findings achieved over the surrounding areas in the eastern Mediterranean basin such as in Israel and Gaza-Strip, as pointed out by Yosef *et al.* (2009), Ziv *et al.* (2013) and Ajjur and Riffi (2020). This positive trend, however, may contribute to increase the occurrence of flash floods especially over the southern Sinai, where the trends were found to be more robust along with a higher evelation gradient (see Fig. 1). Besides, with respect to the temporal rainfall regime of the Sinai, as shown in Figure 3, it was found that the highest ratios of the monthly precipitation from the total annual, occur in early winter; yet mostly limited to the northern Sinai. This, denotes that the remaining months could experience a mild-to-severe prolonged dry-weaether condition throughout the year. From a spatial perspective, we also found that precipitation climatologies are quite unevenly distributed across the Sinai. So that, the norht/northeastern parts receive the highest (>100 mm/year) and south/southwest receive the lowest (<30 mm/year) amounts of precipitation (Fig. 4a). Using the monthly frequency of rainfalls in the Sinai (Fig. 5), we determined the wet-period (October-March) and dry-period (April-September) in the Sinai. Although, a profound dissimilarity was found in the monthly precipitation values during the wet and dry periods (ranging from 5-70mm/month to 1-3mm/month, respectively); however, thier spatial patterns were largely resemblance, meaning that the rainfall amounts are notably increased from the south towards northeast of the Sinai region during both periods (Fig. S7).

Our synoptic analysis (Fig. 7) was conducted to explore the association of the synoptic systems to the precipitation occurrance over the Sinai during the wet –and dry periods (2001-2020). Basically, majority of the cyclones (rainy systems) affecting the study area are generated within the Mediterraniean basin itself and the nearby regions, which spatiotemporally are smaller and have shorter lifetimes compared to those of the north Atlantic systems; a similar result was also reported by Trigo *et al.* (1999) and Buzzi *et al.* (2005). Yet, they are capable of inducing extreme precipitation events and floods in some cases (Homar *et al.,* 2007). Accordingly, we also found that during wet period (Fig. 12a), two major sources of cyclonic activities (cyclogenesis) are responsible for majority of the rainfall events over the region; these are located in the westen part (at the lee of Alps Mountains over Gulf of Genoa) and eastern part (at the lee of Taurus Mountains over Cyprus) of the Mediterranean Sea. The cyclones formed over the Cyprus alegedly play a significant role in the occurrence of rainfalls over the eastern Mediterranean (Saaroni *et al.,* 2010). Besides, another key synoptic system that plays a secondary role in the eastern Mediterranean's rainfall

https://doi.org/10.5194/esd-2022-10
Preprint. Discussion started: 25 March 2022

during the wet period is the Red Sea Trough, which is developed as a result of the coexistance of the Sudan's Low and Saudi Arabia's Anticyclone (see Fig. 12a). However, allegedly the Red Sea Trough has a limited contribution to the Sinai's rainfall comapred to the northeastern parts of the Mediterranean basin such as over Israel (Saaroni *et al.,* 1998, and Tsvieli and Zangvil, 2005). However, during the dry period (Fig. 12b), the number of the Mediterranean's cyclones are significantly reduced (see Fig. 11b) due to the predominance of the high-pressure systems extending from the north Atlantic and north of Africa. This situation largely prevents the rising of air and, in turn, condensation, which all limit rainfall genesis over the region during the dry period. However, as the result of the northwestwards extension of the Persian Trough into the eastern Mediterranean basin, limited cyclones develop and produce rainfalls over the eastern Mediterranean (Alpert *et al.,* 1990; Saaroni and Ziv 2000) including the Sinai region, as shown in Fig. 12b.

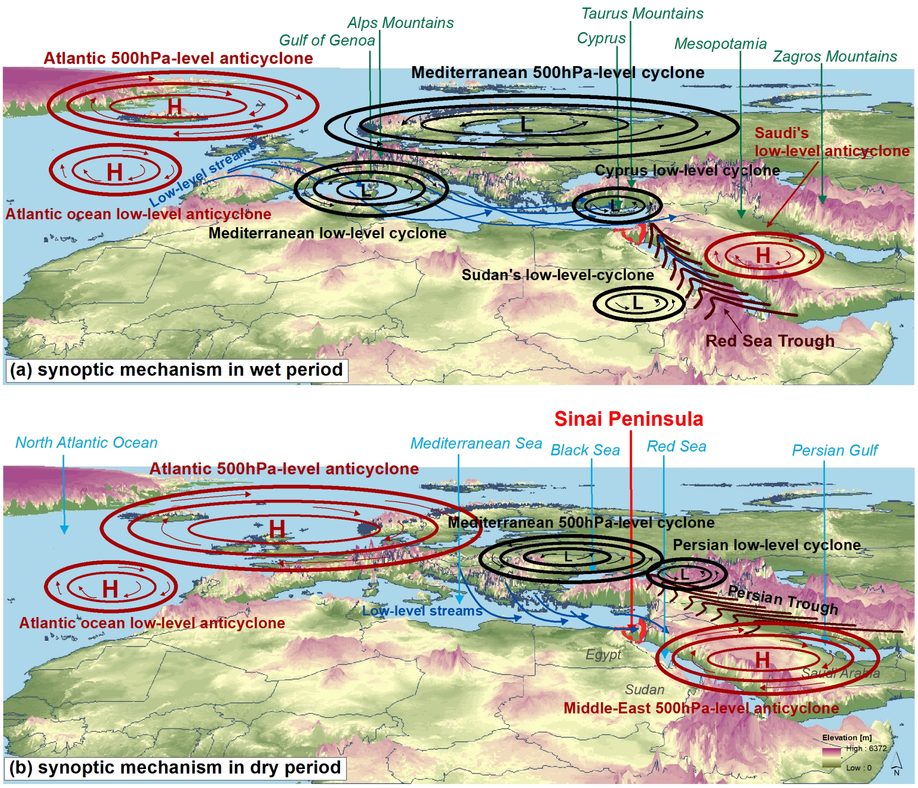

Figure 12. Schematic representation of the dominant synoptic systems corresponding for the Sinai precipitation events (-and also the eastern Mediterranean region) in: (a) wet-period from October to March and (b) dry-period from April to September for the climatology period of 2001-2020.

With respect to the relationships of the Sinai's rainfall against key regional atmospheric variables (Figs. 9 and 10), we found meaningful correlations amongst, but varied remarkably during the wet and dry periods. In this context, a special coupling-correlation pattern was observed between the Sinai's rain against U-wind and V-wind components in wet period (Figs. 10a and 10c). However, despite a strong association between rainfall and atmospheric variables, their correlation coefficients were found to be relatively low (< ±0.3). A couple of major controlling factors, among others, could explain these low r-values. First, a long timeseries of the variables in each episode (>3600 days), and second, a very low rate of annual rainfall over the Sinai (on average 10-100 mm/year). Regarding the former, for instance, we did examine with fewer timeseries (e.g. 100 days), then r-values doubled (-or tripled in some cases). Therefore, seemingly with a longer timeseries, more smoothed correlation coefficients are expected. It is also noted that we found that the magnitude of correlations in the dry period are notably high. This could be explained by a semi-stationary structure of the pressure systems over the region, which despite a

https://doi.org/10.5194/esd-2022-10
Preprint. Discussion started: 25 March 2022

low numbers of rainy-days, play a crucial role in increase of r-values of the dry period compared to those of in the wet period. This implies that, allegedly presence of the low-pressure patterns at low atmospheric levels over the eastern Mediterranean during the dry period of the year are well associated with lower precipitation.

Finally, a daily track of cyclones precipitated over the Sinai region (≥10mm/day) was drawn separately for the wet period (125 cyclones, Fig. 11a) and the dry period (31 cyclones, Fig. 11b). All cyclones were classified into five categories (see Table 2) based on the total rainfall received across the Sinai. Basically, the occurrence and frequency of precipitation events in the eastern Mediterranean (including the Sinai) are largely associated with the passage of cyclonic systems (Ulbrich *et al.,* 2012), of which most of the cyclones are generated within the Mediterranean basin in particular during the winter season (Campins *et al.,* 2000; Nissen *et al.,* 2010) (see Fig. 11a). Amongst, some cyclones are capable of inducing extreme precipitation and floods in the region (Buzzi *et al.,* 2005; Homar *et al.,* 2007). We found that about 15% of the cyclones (rainfall >40mm/day) in the wet period are potentially able to produce torrential rainfalls leading to flash floods over the Sinai. Unlike the wet period (Fig. 11a), both number of cyclones (from 125 to 31) and their magnitudes (from 5 to 2 categories) reduced significantly in dry period (Fig. 11b). Considering the monthly frequency of the cyclones passing through the region, during the wet period (Fig. 11a) February receives the highest numbers of cyclones with 26 out of 125 (20.8%), and followed by January (No. 25, 20%), December (No. 24, 19.2%), March (No. 21, 16.8%), November (No. 16, 12.8%), and finally October with the lowest number of 13 (10.4%). We also found that the cyclone of March 12, 2020 was the most significant torrential rainy-system (>70mm/day) ever occurred in the Sinai region (and perhaps in the surrounding areas) over the past two decades. This is followed by the second extremist one occurred on December 27, 2006 with more than 62mm/day rainfall over the Sinai. The monthly frequency of cyclones during the dry period also showed that April was by far the first with a total number of 20 out of 31 (65%), followed by May (No. 9, 29%), September (No. 2, 6%), and with a zero number for the rest of months (i.e. June, July and August). Amongst, cyclones of April 5, 2006 (27mm/day) and September 30, 2012 (24mm/day) were found to be the extreme ones, respectively.

5 Conclusions

The satellite remote-sensing precipitation (GPM) and reanalysis data (NCEP/NCAR) were employed in the present research to explore the extreme precipitation characteristics over the Sinai Peninsula for the climatology period of 2001-2020. This was achieved by i) quantifying the anomaly, monthly regime, frequency and spatial patterns of the extreme rainfall events, ii) investigating the synoptic-scale systems responsible for the occurrence of rainfalls, and iii) determining the major tracks of cyclones during the wet and dry periods. The key findings are therefore summarized into three major pillars:

i. *Spatiotemporal characteristics of rainfall:* annual/interannual precipitation trends did not show a spatial coherency across the Sinai; rather indicated a spatially dependency. The precipitation regimes also revealed that high ratios of annual rainfalls are mostly received in the early winter. Further, precipitation climatology of the Sinai indicated northeast and southwest of the region receive in order the highest (>100mm/year) and the lowest (<30mm/year) annual rainfall. Also, the distribution of extreme rainfall frequencies, regardless of their thresholds, resembled. This means that highest and lowest frequencies occur from January to March (wet period), and from April to September (dry period), respectively.
ii. *Synoptic atmospheric systems:* majority of cyclones precipitating over the Sinai are generated within the Mediterranean basin (at leeward of the Alps and Taurus Mountains over Gulf of Genoa and Cyprus, respectively), accompanied by the Red Sea Trough at lower-levels during the wet period. These systems either are absent- or weakened significantly during dry period of the region; however, limited low-systems are developed as the result of the Persian Trough extending northwestwards. Further, the spatial correlations of the Sinai's rainfall against key regional variables at multiple levels of the atmosphere revealed meaningful correlation patterns, varied largely in wet and dry periods. Amongst, the relationship of Sinai's rainfall against SLP, U-V winds and vertical velocity was remarkable.
iii. *Cyclone tracking:* A total number of 125 and 31 cyclones (rainfall ≥10mm/day) was tracked during wet and dry periods, respectively. Amongst, 75% of the cyclones produced precipitation ranged 10-30mm/day; while about 15% generated torrential rainfall with >40mm/day, being capable of leading to flash floods in the wet period of the Sinai. However, both frequency (from 125 to 31 cyclones) and magnitude (from 5 to 2 classes) of the cyclones reduced during the dry period as compared to those occurring during the wet season.

Code and data availability. A set of climate functions/indices computed using the Climate Data Operator (CDO) developed at the Max-Planck-Institute for Meteorology are available at: https://code.mpimet.mpg.de/projects/cdo. The satellite GPM and NCEP/NCAR reanalysis datasets used are publicly available at: https://gpm.nasa.gov/ and https://psl.noaa.gov/data/gridded/data.ncep.reanalysis.html, respectively.

Supplement. The supplement related to this article is available online at: (*will be added by the journal*)

Author contributions. MS, BH, AM, SCD, TH, JA and PL designed the study. MS, AM, SCD and PL developed the research goals, and MS wrote the initial manuscript. MS and AM designed and produced the figures and tables. All authors contributed to the interpretation of results and improvement of the manuscript.

Acknowledgements. This research was financially supported by the European centre of excellence for sustainable water technology (Wetsus). The authors would like to acknowledge the Max-Planck-Institute for Meteorology for developing the CDO-tool's functions used in this study to estimate a set of climate indices. A special thanks goes to the NASA/Goddard Space Flight Center for providing the GPM-IMERG (V06B) satellite rainfall data. We also gratefully appreciate the NOAA-NCEP/NCAR reanalysis dataset used in this research.

References

Alpert, P., and Ziv, B.: The Sharav cyclone: Observations and some theoretical considerations. J. Geophys. Res., 94, 18 495–18 514, https://doi.org/10.1029/JD094iD15p18495. 1989.

Alpert, P., Abramsky, R., Neeman, B.U.: The prevailing summer synoptic system in Israel - Subtropical High, not Persian Trough. *Isr J Earth Sci*, 39, 93-102. 1990.

Alpert, P., and Shay-El, Y.: The moisture source for the winter cyclones in the eastern Mediterranean. Israel Meteorological Research Papers (IMRP), 5, 20-27, 1994.

Alpert, P., Ben-Gai, T., Baharad, A., Benjamini, Y., Yekutieli, D., Colacino, M., Diodato, L. Ramis, C., Homar, V., Romero, R., Michaelides, S., Manes, A.: The paradoxical increase of Mediterranean extreme daily rainfall in spite of decrease in total values. Geophysical Research Letters, 29(10), 1536, 10.1029/2001GL013554, 2002.

Alpert, P., Osetinsky, I., Ziv, B., Shafir, H.: Semi-objective classification for daily synoptic systems: application to the eastern Mediterranean climate change. *Int. J. Climatol.* 24:1001-1011, DOI: 10.1002/joc.1036. 2004.

Ajjur, S., and Riffi, M.: Analysis of the observed trends in daily extreme precipitation indices in Gaza Strip during 1974-2016. *Int J Climatol*. 2020;1-12. DOI: 10.1002/joc.6576. 2020.

Almazroui, M., Awad, A.M., Nazrul Islam, M., Al-Khalaf, A.K.: A climatological study: wet season cyclone tracks in the East Mediterranean region. *Theor Appl Climatol*., DOI 10.1007/s00704-014-1178-z. 2014.

Almazroui, M., and Awad, A.M.: Synoptic regimes associated with the eastern Mediterranean wet season cyclone tracks. *Atmospheric Research.* 180, 92-118. http://dx.doi.org/10.1016/j.atmosres.2016.05.015. 2016.

Almazroui, M., Awad, A.M., Nazrul Islam, M.: Characteristics of the internal and external sources of the Mediterranean synoptic cyclones for the period 1956-2013. *Theor Appl Climatol.* 133, 811-827. DOI 10.1007/s00704-017-2218-2. 2017.

Arnous, M.O. and Omar, A.E.: Hydrometeorological hazards assessment of some basins in Southwestern Sinai area, Egypt. Journal of Coastal Conservation. 22:721-743 https://doi.org/10.1007/s11852-018-0604-2. 2018.

Baldi, M., Amin, D., Al Zayed, I.S., Dalu, G.: Climatology and Dynamical Evolution of Extreme Rainfall Events in the Sinai Peninsula-Egypt. Sustainability 2020, 12, 6186; doi:10.3390/su12156186. 2020.

Badreldin, N., and Goossens, R.: A satellite-based disturbance index algorithm for monitoring mitigation strategies effects on desertification change in an arid environment. *Mitig Adapt Strateg Glob Change*. https://doi.org/10.1007/s11027-013-9490-y. 2013.

Barkhordarian, A., von Storch, H., Bhend, J.: The expectation of future precipitation change over the Mediterranean region is different from what we observe. *Clim Dyn.* 40:225–244. DOI 10.1007/s00382-012-1497-7. 2013.

Ben David-Novak, H., Morin, E., Enzel, Y.: Modern extreme storms and the rainfall thresholds for initiating debris flows on the hyperarid western escarpment of the Dead Sea, Israel. Geological Society of America Bulletin, May/June 2004; v. 116; no. 5/6; p. 718-728; doi: 10.1130/B25403.1. 2004.

https://doi.org/10.5194/esd-2022-10
Preprint. Discussion started: 25 March 2022

Ben-Zvi, A.: Rainfall intensity-duration-frequency relationships derived from large partial duration series. *Journal of Hydrology* 367, 104-114. doi:10.1016/j.jhydrol.2009.01.007. 2009.

Boucek, R.E., Gaiser, E.E., Liu, H., and Rehage, J.S.: A review of subtropical community resistance and resilience to extreme cold spells, Ecosphere, 7(10), e01455, https://doi.org/10.1002/ecs2.1455. 2016.

Buzzi, A., Richard, E., Romero, R.: Summary Report on MEDEX Studies and Scientific Results on Mediterranean Cyclones Causing High Impact Weather. MEDEX Project http://medex.aemet.uib.es/index.html. 2005.

Campins, J., Genoves, A., Jansa, A., Guijarro, J.A., Ramis, C.: A catalogue and a classification of surface cyclones for the western Mediterranean. *Int J Climatol*, 20, 969-984. 2000.

Caracciolo, D., Francipane, A., Viola, F., Valerio Noto, L., Deidda, R.: Performances of GPM satellite precipitation over the two major Mediterranean islands. *Atmospheric Research*. 213 (15), 309-322. https://doi.org/10.1016/j.atmosres.2018.06.010. 2018.

Charlton-Perez, A.J., Aldridge, R.W., Grams, C.M., and Lee, R.: Winter pressures on the UK health system dominated by the Greenland blocking weather regime, Weather and Climate Extremes, 25, 100218, https://doi.org/10.1016/j.wace.2019.100218. 2019.

Cinzia Marra, A., Federico, S., Montopoli, M., Avolio, E., Baldini, L., Casella, D., D'Adderio, L.P., Dietrich, S., Sanò, P., Torcasio, R.C, Panegrossi, G.: The Precipitation Structure of the Mediterranean Tropical-Like Cyclone Numa: Analysis of GPM Observations and Numerical Weather Prediction Model Simulations. *Remote Sens.* 2019, 11, 1690; doi:10.3390/rs11141690. 2019.

Cools, J., Vanderkimpen, P., El Afandi, G., Abdelkhalek, A., Fockedey, S., El Sammany, M., Abdallah, G., El Bihery, M., Bauwens, W., Huygens, M.: An early warning system for flash floods in hyper-arid Egypt. *Nat. Hazards Earth Syst. Sci.,* 12, 443–457. doi:10.5194/nhess-12-443. 2012.

David-Novak, H.B., Morin, E., and Enzel, Y.: Modern extreme storms and the rainfall thresholds for initiating debris flows on the hyperarid western escarpment of the Dead Sea Israel, GSA Bulletin, 116(5/6), 718–728, https://doi.org/10.1130/B25403.1. 2004.

Dayan, U., Ziv, B., Margalit, A., Morin, E. Sharon, D.: A severe autumn storm over the middle-east: synoptic and mesoscale convection analysis. *Theor. Appl. Climatol*. 69, 103-122. 2001.

Dayan, U., Nissen, K., Ulbrich, U.: Review Article: Atmospheric conditions inducing extreme precipitation over the eastern and western Mediterranean. *Nat. Hazards Earth Syst. Sci., 15, 2525-2544, 2015*. doi:10.5194/nhess-15-2525-2015. 2015.

Dadamouny, M.A., Schnittler M.: Trends of climate with rapid change in Sinai, Egypt. Journal of Water and Climate Change, 7.2, 393-414. doi: 10.2166/wcc.2015.215. 2016.

de Vries, A.J., Tyrlis, E., Edry D., Krichak, S.O., Steil, B., Lelieveld, J.: Extreme precipitation events in the Middle East: Dynamics of the Active Red Sea Trough. *Journal of Geophysical Researches*.118, 7087-7108, doi:10.1002/jgrd.50569, 2013.

El-Magd, A.I., Hermas, E., El-Bastawesy, M.: GIS modelling of the spatial variability of flash flood hazard in Abu Dabbab Catchment, Red Sea Region, Egypt. Egypt J Remote Sens Sp Sci 13:81-88. 2010.

El Afandi, G., Morsy, M., El Hussieny F.: Heavy Rainfall Simulation over Sinai Peninsula Using the Weather Research and Forecasting Model. International Journal of Atmospheric Sciences, 241050, 11. http://dx.doi.org/10.1155/2013/241050. 2013.

El-Fakharany, M.A., and Mansour, N.M.: Morphometric analysis and flash foods hazards assessment for Wadi Al Aawag drainage Basins, southwest Sinai, Egypt. Environmental Earth Sciences, 80:168 https://doi.org/10.1007/s12665-021-09457-1. 2021.

El-Sayed, E.A, and Habib, E.: Advanced Technique for Rainfall-Runoff Simulation in Arid Catchments Sinai, Egypt. The 3rd International Conf. on Water Resources & Arid Environment (2008) and First Arab Forum. 2008.

Farahat, M.S., Elmoustafa, A.M., Hasan, A.A.: Developing flash foods inundation maps using remote sensing data, a case study: Wadi AL-Arish, Sinai, Egypt. Am J Eng Res (AJER) 6(5):172-181. 2017.

Flocas, H., Simmonds, L., Kouroutzoglou, J., Keay, K., Hatzaki, M., Bricolas, V., Asimakopoulos, D.: On Cyclonic Tracks over the Eastern Mediterranean. Journal of Climate, 23, 5243-5257, DOI: 10.1175/2010JCLI3426.1. 2010.

Flaounas, E., Kotroni, V., Lagouvardos, K., Gray, S., Rysman, J.F., Claud, C.: Heavy rainfall in Mediterranean cyclones, Part I: Contribution of deep convection and warm conveyor. *Climate Dynamics,* 50 (7 8), 2935-2949, doi: https://doi.org/10.1007/s003820173783x. 2014a.

Flaounas, E., Raveh-Rubin, S., Wernli, H., Drobinski, P., Bastin, S.: The dynamical structure of intense Mediterranean cyclones. *Climate Dynamics,* DOI 10.1007/s00382-014-2330-2. 2014b.

Gado T.A.: Statistical Behavior of Rainfall in Egypt. In: Negm A. (eds) Flash Floods in Egypt. Advances in Science, Technology & Innovation (IEREK Interdisciplinary Series for Sustainable Development). Springer, Cham. https://doi.org/10.1007/978-3-030-29635-3_2. 2020.

Givati, A., Thirel, G., Rosenfeld, D., Paz, D.: Climate change impacts on streamflow at the upper Jordan River based on an ensemble of regional climate models. Journal of Hydrology: Regional Studies 21, 92-109, https://doi.org/10.1016/j.ejrh.2018.12.004. 2019.

Gabella, M., Michaelides, S., Constantinides, P., Perona, G.: Climatological validation of TRMM precipitation radar monthly rain products over Cyprus during the first 5 years (December 1997 to November 2002). Meteorol. Z. 15 (5), 559-564. 2006.

Hochman, A., Rostkier-Edelstein, D., Kunin, P., Pinto, J.G.: Changes in the characteristics of 'wet' and 'dry' Red Sea Trough over the Eastern Mediterranean in CMIP5 climate projections. *Theoretical and Applied Climatology*, 143, 781-794, https://doi.org/10.1007/s00704-020-03449-0. 2020.

Homar, V., Jansa, A., Campins, J., Genoves, A., Ramis, C.: Towards a systematic climatology of sensitivities of Mediterranean high impact weather: a contribution based on intense cyclones, *Nat. Hazards Earth Syst. Sci*., 7, 445-454.2007.

Hourngir, D., Panegrossi, G., Casella, D., Sanò, P., D'Adderio, L.P., Liu, C.: A 4-Year Climatological Analysis Based on GPM Observations of Deep Convective Events in the Mediterranean Region. *Remote Sens.* 2021, 13, 1685. https://doi.org/10.3390/rs13091685. 2021.

Huffman, G.J., Bolvin, D.T., Braithwaite, D., Hsu, K., Joyce, R., Xie, P.: NASA Global Precipitation Measurement (GPM) Integrated Multi-satellitE Retrievals for GPM (IMERG), NASA Report, 1-35, 2014.

IPCC Climate Change: The Physical Science Basis. Contribution of Working Group I to the Fifth Assessment Report of the Intergovernmental Panel on Climate Change [Stocker TF. Qin D. Plattner GK. Tignor M. Allen SK. Boschung J. Nauels A. Xia Y. Bex V. and Midgley PM. (eds.)]. Cambridge University Press, Cambridge, United Kingdom and New York, NY, USA, 1535 pp, 2013.

Kahana, R., Ziv, B., Enzel, Y., Dayan, U.: Synoptic climatology of major floods in the Negev desert, Israel. *Int. J. Climatol.* 22: 867-882. DOI: 10.1002/joc.766. 2002.

Kalnay, E., et al.: The NCEP/NCAR 40-year reanalysis project. Bull Am Meteorol Soc 77:437-471. 1996.

Koutroulis, A.G., and Tsanis, I.K.: A method for estimating flash flood peak discharge in a poorly gauged basin: Case study for the 13–14 January 1994 flood, Giofiros basin, Crete, Greece. *Journal of Hydrology* 385, 150-164. doi:10.1016/j.jhydrol.2010.02.012. 2010.

Kostopoulou, E., and Jones, P.D.: Assessment of climate extremes in the Eastern Mediterranean. *Meteorol Atmos Phys* 89, 69-85. DOI 10.1007/s00703-005-0122-2. 2005.

Kotsias, G., Lolis, C., Hatzianastassiou, N., Lionello, P., Bartzokas, A.: An objective definition of seasons for the Mediterranean region. *Int J Climatol*. 2020;1-17. DOI: 10.1002/joc.6819. 2020.

Kotroni, V., Lagouvardos, K., Defer, E.: The Antalya 5 December 2002 Storm: Observations and Model Analysis. *Journal of Applied Meteorology and Climatology*. 45, 576-590.https://doi.org/10.1175/JAM2347.1.2006.

Krichak, S.O., Kishcha P., Alpert, P.: Decadal trends of main Eurasian oscillations and the Eastern Mediterranean precipitation. *Theor. Appl. Climatol.* 72, 209-220. 2002.

Krichak, S.O., Alpert, P., Krishnamurti, T.N.: Red Sea Trough/Cyclone Development- Numerical Investigation. *Meteorol, Atmos. Phys.* 63, 159-169. 1997.

Levy, Y., Burg, A., Yechieli, Y., Gvirtzman, H.: Displacement of springs and changes in groundwater flow regime due to the extreme drop in adjacent lake levels: The Dead Sea rift. J. Hydrol., 587, 124928, https://doi.org/10.1016/j.hydrol.2020.124928. 2020.

Lionello, P., Trigo, I., Gil, V., Liberato, M.R., et al.: Objective climatology of cyclones in the Mediterranean region: a consensus view among methods with different system identification and tracking criteria. Tellus A 2016, 68, 29391, http://dx.doi.org/10.3402/tellusa.v68.29391. 2016.

Lois, C.J.: Winter cloudiness variability in the Mediterranean region and its connection to atmospheric circulation features. *Theor Appl Climatol*., 96:357-373. DOI 10.1007/s00704-008-0046-0. 2009.

Mathbout, S., Lopez-Bustins, A., Roye, D., Martin-Vide, J., Bech J., Rodrigo, F.S.: Observed Changes in Daily Precipitation Extremes at Annual Timescale Over the Eastern Mediterranean During 1961-2012. Pure Appl. Geophys. 175, 3875-3890. https://doi.org/10.1007/s00024-017-1695-7. 2018.

https://doi.org/10.5194/esd-2022-10
Preprint. Discussion started: 25 March 2022

Earth System Dynamics
Discussions

Morsy, M., Sayad, T., Khamees, A.S.: Towards instability index development for heavy rainfall events over Egypt and the Eastern Mediterranean. *Meteorology and Atmospheric Physics*, 132, 255-272, https://doi.org/10.1007/s00703-019-00686-5. 2019.

Mehta, A.V., and Yang, S.: Precipitation climatology over Mediterranean Basin from ten years of TRMM measurements. Adv. Geosci. 17, 87-91. https://doi.org/10.5194/adgeo-17-87-2008. 2008.

Morin, E., Harats, N., Jacoby, Y., Arbel, S., Getker, M., Arazi, A., Grodek, T., Ziv, B., Dayan, U.: *Adv. Geosci.,* 12, 107-114, 2007. www.adv-geosci.net/12/107/2007. 2007.

Mohamed, S.A., and El-Raey, M.E.: Vulnerability assessment for flash foods using GIS spatial modeling and remotely sensed data in El-Arish City, North Sinai, Egypt. *Natural Hazards*, 102, 707-728, https://doi.org/10.1007/s11069-019-03571-x. 2019.

Morad, N.A.: Assessment of the rainfall storm events of January 2010 and March 2014 for the catchment modelling of Wadi-El-Arish and Wadi-Wardan basins, Sinai, Egypt. *Egyptian J. Desert Res.,* 66, No. 1, 137-168 (2016). 2016.

Nastos, P.T., Kapsomenakis, J., Douvis, K.C.: Analysis of precipitation extremes based on satellite and high-resolution gridded data set over Mediterranean basin. *Atmospheric Research* 131, 46-59. http://dx.doi.org/10.1016/j.atmosres.2013.04.009. 2013.

Neu, U., Akperov, M.G., Bellenbaum, N., Benestad, R., et al.: IMILAST: A Community Effort to Intercompare Extratropical Cyclone Detection and Tracking Algorithms. *Bulletin of the American Meteorological Society*, 94(4), 529-547. DOI: https://doi.org/10.1175/BAMS-D-11-00154.1. 2013.

Nissen, K.M., Leckebusch, G.C., Pinto, J.G., Renggli, D., Ulbrich, S., Ulbrich, U.: Cyclones causing wind storms in the Mediterranean: characteristics, trends and links to large-scale patterns. *Nat Hazards Earth Syst Sci*, 10, 1379-1391. 2010.

Ocakoglu, F., Gokceoglu, C., Ercanoglu, M.: Dynamics of a complex mass movement triggered by heavy rainfall: a case study from NW Turkey. Geomorphology, 42, 329, 341, 2002.

Omran, E.-S.E.: Egypt's Sinai Desert Cries: Flash Flood Hazard, Vulnerability, and Mitigation. Springer Nature Switzerland AG 2020 A.M. Negm (ed.), Flash Floods in Egypt, Advances in Science, Technology & Innovation, https://doi.org/10.1007/978-3-030-29635-3_11. 2020.

Petracca, M., D'Adderio, L.P., Porcu, F., Vulpiani, G., Sebastianelli, S., Puca S.: Validation of GPM Dual-Frequency Precipitation Radar (DPR) Rainfall Products over Italy. *Journal of Hydrometeorology*, 19, 907-925. DOI: 10.1175/JHM-D-17-0144.1. 2018.

Prama, M., Omran, A., Schröder, D., Abouelmagd, A.: Vulnerability assessment of flash floods in Wadi Dahab Basin, Egypt. Environmental Earth Sciences, 79:114. https://doi.org/10.1007/s12665-020-8860-5. 2020.

Peleg, N., and Morin, E.: Convective rain cells: Radar-derived spatiotemporal characteristics and synoptic patterns over the eastern Mediterranean. *Journal of Geophysical Research*, 117, D15116, doi:10.1029/2011JD017353, 2012. 2012.

Peleg, N., Morin, E., Gvirtzman, H., Enzel, Y.: Rainfall, spring discharge and past human occupancy in the Eastern Mediterranean. Clim. Change 112(3-4): 769-789, https://doi.org/10.1007/s10584-011- 0232-4. 2012.

Pfahl, S., and Wernli, H.: Quantifying the relevance of atmospheric blocking for co-located temperature extremes in the Northern Hemisphere on (sub-)daily time scales. 39(12), L12807. https://doi.org/10.1029/2012GL052261. 2012.

Retalis, A., Katsanos, D., Tymvios, F., Michaelides, S.: Validation of the First Years of GPM Operation over Cyprus. *Remote Sens.* 2018, 10, 1520; doi:10.3390/rs10101520. 2018.

Romera, R., Gaertner, M.A., Sánchez, E., Domínguez, M., González-Alemán, J.J., Miglietta, M.M.: Climate change projections of medicanes with a large multi-model ensemble of regional climate models. *Global and Planetary Change,* 2016, http://dx.doi.org/10.1016/j.gloplacha.2016.10.008. 2016.

Rinat, Y., Marra, F., Armon, M., Metzger, A., Levi, Y., Khain, P., Vadislavsky, E., Rosensaft, M., Morin, E.: Hydrometeorological analysis and forecasting of a 3 d flash-flood-triggering desert rainstorm. *Nat. Hazards Earth Syst. Sci.,* 21, 917-939, 2021. https://doi.org/10.5194/nhess-21-917-2021. 2021.

Raveh-Rubin, S., and Wernli, H.: Large-scale wind and precipitation extremes in the Mediterranean: a climatological analysis for 1979–2012. *Q. J. R. Meteorol. Soc.* 141, 2404-2417. 2015.

Roushdi, M., Mostafa, H., Kheireldin, K.: Present and future climate extreme indices over Sinai Peninsula, Egypt. World academy of science, engineering and technology. Int J Geol Environ Eng 109:85-90. 2016.

Saaroni, H., Ziv, B., Bitan, A., Alpert, P.: Easterly wind storms over Israel. Theor Appl Climatol, 59, 61-77. 1998.

https://doi.org/10.5194/esd-2022-10
Preprint. Discussion started: 25 March 2022

Saaroni, H., Ziv, B.: Summer rain episodes in a Mediterranean Climate, the case of Israel: climatological-dynamical analysis. *Int J Climatol*, 20, 191- 209. 2000.

Saaroni, H., Halfon, N., Ziv, B., Alpert, P., Kutiel, H.: Links between the rainfall regime in Israel and location and intensity of Cyprus lows. Int J Climatol, 30, 1014-1025. 2010.

Shohami, D., Dayan, U., Morin, E.: Warming and drying of the eastern Mediterranean: Additional evidence from trend analysis. *Journal of Geophysical Research*, 116, D22101. doi:10.1029/2011JD016004. 2011.

Schulzweida, U.: CDO User Guide (V. 1.9.9). Zenodo. http://doi.org/10.5281/zenodo.4246983. 2020.

Samuels, R., Rimmer, A., Alpert, P.: Effect of extreme rainfall events on the water resources of the Jordan River. *Journal of Hydrology* 375, 513-523. doi:10.1016/j.jhydrol.2009.07.001. 2009.

Spyrou, C., Varlas, G., Pappa, A., Mentzafou, A., Katsafados, P., Papadopoulos, A., Anagnostou, M.N., Kalogiros, J.: Implementation of a Nowcasting Hydrometeorological System for Studying Flash Flood Events: The Case of Mandra, Greece. *Remote Sens.* 2020, 12, 2784; doi:10.3390/rs12172784. 2020.

Tolika, K., Maheras, P., Flocas, H.A., Arseni-Papadimitriou, A.: An evaluation of a general circulation model (GCM) and the NCEP-NCAR reanalysis data for winter precipitation in Greece. *Int. J. Climatol.* 26: 935-955. DOI: 10.1002/joc.1290. 2006.

Toreti, A., Giannakaki, P., Martius, O.: Precipitation extremes in the Mediterranean region and associated upper-level synoptic-scale flow structures. *Clim Dyn*, 47:1925-1941. DOI 10.1007/s00382-015-2942-1. 2016.

Tsvieli, Y., and Zangvil, A.: Synoptic climatological analysis of wet and dry Red Sea toughs over Israel. *Int. J. Climatol.* 25: 1997-2015. DOI: 10.1002/joc.1232. 2005.

Trenberth KE, Jones PD, Ambenje P, Bojariu R, Easterling D, Klein Tank A, Parker D, Rahimzadeh F, Renwick JA, Rusticucci M, Soden B, Zhai P.: Observations: surface and atmospheric climate change. In Climate Change 2007: The Physical Science Basis. Contribution of Working Group 1 to the Fourth Assessment Report of the Intergovernmental Panel on Climate Change, Solomon S, Qin D, Manning M, Chen Z, Marquis M, Averyt KB, Tignor M, Miller HL (eds). Cambridge University Press: Cambridge and New York, NY; 235–336. 2007.

Tarolli, P., Borga, M., Morin, E., Delrieu, G.: Analysis of flash flood regimes in the North-Western and South-Eastern Mediterranean regions. *Nat. Hazards Earth Syst. Sci.,* 12, 1255-1265, 2012. www.nat-hazards-earth-syst-sci.net/12/1255/2012. 2012.

Trigo, I.F., Davies, T.D., Bigg, G.R.: Objective climatology of cyclones in the Mediterranean region. *J Climate*, 12, 6, 1685-1696. 1999.

Trigo, I., Bigg, G.R., Davies, T.D.: Climatology of Cyclogenesis Mechanisms in the Mediterranean. *Monthly Weather Review*, 130, 549-569. 2002.

Trigo, R.M., Trigo, I.F., DaCamara, C.C.: Climate impact of the European winter blocking episodes from the NCEP/NCAR Reanalyses. *Climate Dynamics*, 23: 17-28. DOI 10.1007/s00382-004-0410-4. 2004.

Trigo, I.F.: Climatology and interannual variability of storm-tracks in the Euro-Atlantic sector: a comparison between ERA-40 and NCEP/NCAR reanalyses. *Climate Dynamics*, 26: 127-143. DOI 10.1007/s00382-005-0065-9. 2006.

Tous, M., Zappa, G., Romero, R., Shaffrey, L., Vidale, P.L.: Projected changes in medicanes in the HadGEM3 N512 high-resolution global climate model. *Clim Dyn*, 47:1913-1924. DOI 10.1007/s00382-015-2941-2. 2015.

Toros, H., Kahraman, A., Tilev-Tanriover, S., Geertsema, G., Cats, G.: Simulating Heavy Precipitation with HARMONIE, HIRLAM and WRF-ARW: A Flash Flood Case Study in Istanbul, Turkey. *European Journal of Science and Technology*, 13, 1-12, DOI: 10.31590/ejosat.417535. 2018.

Toreti, A., Xoplaki, E., Maraun, D., Kuglitsch, F.G., Wanner, H., Luterbacher, J.: Characterization of extreme winter precipitation in Mediterranean coastal sites and associated anomalous atmospheric circulation patterns. *Nat. Hazards Earth Syst. Sci.,* 10, 1037-1050, doi:10.5194/nhess-10-1037-2010. 2010.

Ulbrich, U., Lionello, P., Belušic, D., Jacobeit, J., Knippertz, P., Kuglitsch, F.G., et al.,: Climate of the Mediterranean: Synoptic Patterns, Temperature, Precipitation, Winds, and Their Extremes, in book: *The Climate of the Mediterranean Region*, Elsevier, pp.301-346. https://doi.org/10.1016/B978-0-12-416042-2.00005-7. 2012.

Varlas, G., Anagnostou, M., Spyrou, C., Papadopoulos, A., Kalogiros, J., Mentzafou, A., Michaelides, S., Baltas, E., Karymbalis, E., Katsafados, P.: A Multi-Platform Hydrometeorological Analysis of the Flash Flood Event of 15 November 2017 in Attica, Greece. *Remote Sens*. 2019, 11, 45; doi:10.3390/rs11010045. 2018.

https://doi.org/10.5194/esd-2022-10
Preprint. Discussion started: 25 March 2022

Earth System Dynamics
Discussions

Wannous, C., and Velasquez G.,: United Nations Office for Disaster Risk Reduction (UNISDR)-UNISDR's Contribution to Science and Technology for Disaster Risk Reduction and the Role of the International Consortium on Landslides (ICL) Open image in new window In: Sassa K., Mikoš M., Yin Y. (eds) Advancing Culture of Living with Landslides. WLF 2017. Springer, Cham. https://doi.org/10.1007/978-3-319-59469-9_6. 2017.

Yucel, I., and Onen, A.: Evaluating a mesoscale atmosphere model and a satellite-based algorithm in estimating extreme rainfall events in northwestern Turkey. *Nat. Hazards Earth Syst. Sci.,* 14, 611-624, 2014. doi:10.5194/nhess-14-611-2014. 2014.

Yosef, Y., Saaroni, H., Alpert, P.: Trends in Daily Rainfall Intensity Over Israel 1950/1-2003/4. The Open Atmospheric Science Journal, 2009, 3, 196-203. 2009.

Zappa, G., Hawcroft, M.K., Shaffrey, L., Black, E., Brayshaw, D.J.,: Extratropical cyclones and the projected decline of winter Mediterranean precipitation in the CMIP5 models. *Climate Dynamics* 45, 1727-1738 (2015). DOI 10.1007/s00382-014-2426-8. 2014

Zhang, X., Aguilar, E., Sensoy, S., Melkonyan, H., Tagiyeva, U., Ahmed, N., Kutalade, N., Rahimzadeh, F., Taghipour, A,. Hantosh, T.H., Alpert, P., Semawi, M., Ali, M.K., Al-Shabibi, M.H.S., Al-Oulan, Z., Zatari, T., Khelet, I.A.D., Hamoud, S., Sagir, R., Demircan, M., Eken, M., Adiguzel, M., Alexander, L., Peterson, T.C., Wallis, T.: Trends in Middle East climate indices from 1950 to 2003, J. Geophys. Res. Atmos, 110, D22104, https://doi.org/10.1029/2005JD006181, 2005.

Zittis, G., Bruggeman, A., Camera, C.: 21st Century Projections of Extreme Precipitation Indicators for Cyprus. Atmosphere, 2020, 11, 343; doi:10.3390/atmos11040343. 2020.

Ziv, B., Saaroni, H., Paramount, R., Harpaz, T., Alpert, P.: Trends in rainfall regime over Israel, 1975–2010, and their relationship to large-scale variability. *Reg Environ Change*. DOI 10.1007/s10113-013-0414-x. 2013.

Ziv, B., Harpaz, T., Saaroni, H., Blender, R.: A new methodology for identifying daughter cyclogenesis: application for the Mediterranean Basin. *Int. J. Climatol.* (2015), DOI: 10.1002/joc.4250. 2015.

Ziv, B., Saaroni, H., Etkin, A., Harpaz, T., Shendrik, L.: Formation of cyclones over the East Mediterranean within Red-Sea Troughs. *Int J Climatol*. 2021;1-20. DOI: 10.1002/joc.7261.

Zoccatelli, D., Marra, F., Armon, M., Rinat, Y., Smith, J., Morin, E.: Contrasting rainfall-runoff characteristics of floods in desert and Mediterranean basins. *Hydrol. Earth Syst. Sci.,* 23, 2665-2678. https://doi.org/10.5194/hess-23-2665-2019. 2019.

Zoccatelli, D., Marra, F., Smith, J., Goodrich, D., Unkrich, C., Rosensaft, M., Morin, E.: Hydrological modelling in desert areas of the eastern Mediterranean. *Journal of Hydrology,* 587, 124879. https://doi.org/10.1016/j.jhydrol.2020.124879. 2020.